

Institutionen för systemteknik

Department of Electrical Engineering

Examensarbete

Enhancement Techniques for Lane Position Adaptation (Estimation) using GPS- and Map Data

Examensarbete utfört i sensorfusion
vid Tekniska högskolan vid Linköpings universitet
av

Markus Landberg

LiTH-ISY-EX--14/4788--SE

Linköping 2014



Linköpings universitet
TEKNISKA HÖGSKOLAN

Enhancement Techniques for Lane Position Adaptation (Estimation) using GPS- and Map Data

Examensarbete utfört i sensorfusion
vid Tekniska högskolan i Linköping
av

Markus Landberg

LiTH-ISY-EX--14/4788--SE

Handledare: **Rudolf Mester**
isy, Linköpings universitet

Examinator: **Rudolf Mester**
isy, Linköpings universitet

Linköping, 1 September, 2014

Abstract

A lane position system and enhancement techniques, for increasing the robustness and availability of such a system, are investigated. The enhancements are performed by using additional sensor sources like map data and GPS. The thesis contains a description of the system, two models of the system and two implemented filters for the system. The thesis also contains conclusions and results of theoretical and experimental tests of the increased robustness and availability of the system. The system can be integrated with an existing system that investigates driver behavior, developed for fatigue. That system was developed in a project named Drowsi, where among others Volvo Technology participated.

Sammanfattning

Ett filpositioneringssystem undersöks och förbättringstekniker för ökandet av robusthet och tillgängligheten av ett sådant system genom att använda ytterligare sensorkällor som kartdata och GPS. Detta examensarbete presenterar beskrivningen av ett system, två modeller och två implementerade filter. Examensarbetet innehåller också slutsatser och resultat av teoretiska och experimentella tester som plottar och grafer av ökad robusthet och tillgängligheten av systemet. Detta system kan bli integrerat med ett framtaget system som tittar på körrelaterat beteende vid trötthet. Systemet är utvecklat i ett projekt kallat Drowsi, där bland andra Volvo Technology deltog.

Acknowledgments

I would like to thank Filip Holmqvist and Henrik Wassén at Volvo Technology. Filip for his help with practical arrangements and support during the whole thesis and Henrik for helping me getting started with the thesis and for taking me to Gothenburg and Volvo Technology. Thanks to Björn Svedlund, project manager at ABB in Luleå at the time working for Volvo, who helped me drive the vehicle and helped me connect the equipment to collect data. I am grateful to Post doc Christian Lundquist, Linköping Institute of Technology, for interesting discussions and for coming up with new ideas. I also would like to thank Professor Thomas Schön, Uppsala University and my examiner Professor Rudolf Mester, Linköping Institute of Technology. Further, I would like to thank Professor Svante Gunnarsson, Linköping Institute of Technology, for valuable inputs and help to structure the thesis report. Finally, I would like to thank all colleagues and friends at Volvo Technology for their help and support during the thesis and for making my time there a great time.

Linköping, September 2014

Markus Landberg

Contents

1	Introduction	3
1.1	Background	3
1.2	Volvo Technology Corporation	4
1.3	Problem Specification and Goal	4
1.4	Contributions	5
1.5	Thesis Outline	7
2	Literature Study	9
2.1	Related Work with Positioning Systems using additional Sensor Sources	9
3	Coordinate Systems and Geographical Positions	13
3.1	Models of the Earth	13
3.2	Cartesian, Geocentric and Geodetic Coordinates	14
3.3	Map Projections	15
3.4	Coordinate Frames	17
4	Positioning Techniques Related to This Thesis	19
4.1	Camera	19
4.2	Dead Reckoning	20
4.3	GPS	21
5	Data Collection and Preprocessing	23
5.1	Data Collection	23
5.1.1	Data Sequence 1	24
5.1.2	Data Sequence 2	24
5.1.3	Data from the LPS System	24
5.1.4	Data from Vehicle Sensors	26
5.1.5	Data from the GPS	27
5.1.6	Data from the Swedish National Road Administration	28
5.2	Preprocessing	29
5.2.1	Data from the LPS system	29
5.2.2	Data from the Vehicle Sensors	29
5.2.3	Data from the GPS	29
5.2.4	Data from the Swedish National Road Administration	30

6	Theory	31
6.1	The Linear State Space Model	31
6.2	The Kalman Filter	32
6.3	Overview of the Calculations in the KF	33
6.4	The Nonlinear State Space Model and EKF	34
6.5	Overview of the Calculations in the EKF	36
6.6	Alternative Filters	36
7	Model	39
7.1	Single Track Model with Road Interaction	39
7.2	State Space Model for the complete Lane Positioning System . . .	41
7.2.1	Complete Measurement Equations	42
8	Extended Model	43
8.1	GPS and DR Model	43
8.2	Constant Velocity Model	44
8.3	Coordinated Turn Model	44
8.4	State Space Model for the complete Extended Lane Positioning Sys- tem	45
8.4.1	Complete Extended Measurement Equations	46
9	Results	47
9.1	Technique 1: Curvature and Position Compared with Data from the Swedish National Road Administration	47
9.2	Technique 2: Curvature and Distance Compared with Data from the Swedish National Road Administration	51
9.3	Technique 3: Curvature and Time Compared with the Data from the Swedish National Road Administration	54
9.4	Technique 4: Curvature and Position Compared with Data from the Swedish National Road Administration	57
9.5	Root Mean Square	57
9.6	Summarization of Results	57
10	Conclusions and Future Work	61
10.1	Summary of Conclusions	61
10.2	Future work	62
	Bibliography	65
A	Figures	69
A.1	The raw signal for the whole route	69
A.1.1	Data from GPS	69
A.1.2	Data from the Swedish National Road Administration . . .	70
A.2	The raw signal on a selected interval for the whole route on a road stretch with curves	72
A.2.1	Data from LPS system on a road stretch with curves	72
A.2.2	Data from vehicle sensors	75

A.2.3	Data from GPS	76
A.3	The raw signal on a selected interval for the whole route with disturbance	79
A.3.1	Data from LPS system	79
A.3.2	Data from vehicle sensors	82
A.3.3	Data from GPS	83
B	Figures from technique 4, chapter 9.4	87
B.1	Technique 4	87
B.1.1	Subtechnique T4GPS	87
B.1.2	Subtechnique T4Distance	90
B.1.3	Subtechnique T4Time	93

Notation

Symbols	
α	angular velocity
c_0	road curvature
c_{0R}	the curvature from the lane marking right
c_{0L}	the curvature from the lane marking left
c_1	road curvature derivative
χ	heading angle
χ_R	heading angle right
χ_L	heading angle left
D_k	measurement input matrix
δ_f	mean front wheel angle
δ_k	vehicle constant for the relation between δ_f and δ_s
δ_s	steering wheel angle
δ_s^{offs}	steering wheel angle bias offset
δ_s^m	the measured steering wheel angle
E	East coordinate in UTM
F_k	system matrix
$G_{u,k}$	system input matrix
$G_{w,k}$	process noise matrix
H_k	measurement matrix
K	Kalman gain matrix
l_b	wheel base
l_E	offset between the ego vehicle and the center line
N	North coordinate in UTM
P	covariance matrix of the state estimation error
ψ_E	the ego vehicle's yaw angle
ψ_{RE}	angle between the ego vehicle and the road tangent
Q_k	covariance matrix of the process noise
R	radius
R_k	covariance matrix of the measurement noise
s	distance
t	time
T	sample time
v_k	measurement noise
v_x	longitudinal velocity
W	angular velocity
w	white noise
w_k	process noise
x_{GPS}	x-coordinate of GPS in WGS 84
\hat{x}	estimated state vector
\tilde{x}	state estimation error
y_{GPS}	y-coordinate of GPS in WGS 84
Z	Height coordinate in UTM

Abbreviations	
2D	two dimensional
3D	three dimensional
ABS	Anti-Lock Braking System
BA	Bundle Adjustment
BLUE	Best Linear Unbiased Estimator
CAN	Controller Area Network
CM	Mass Centre of the earth
DDF	Divided Difference Filter
DR	Dead Reckoning
ECEF	Earth Centered Earth Fixed
EKF	Extended Kalman Filter
GIS	Geographical Information Systems
GK	Gauss-Krüger
GNSS	Global Navigation Satellite Systems
GS-KF	Gaussian Sum Kalman Filters
GS-QKF	Gaussian Sum Quadrature Kalman Filter
GUI	Graphical User Interface
GPS	Global Positioning System
HMI	Human-Machine Interaction
INS	Inertial Navigation System
IVT	Intelligent Vehicle Technologies
KF	Kalman Filter
LIDAR	LIght Detection and Ranging
LPS	Lane Position Sensor
MSE	Mean Square Error
NEZ	North East Height
PDF	Probability Density Function
PCS	Personal Communication Systems
PF	Particle Filter
PMF	Point Mass Filter
QKF	Quadrature Kalman Filter
RADAR	RAdio Detection And Ranging
RT90	Swedish grid in swedish Rikets Nät RT90
SfM	Structure from Motion
STM	Single Track Model
STMRI	Single Track Model with Road Interaction
TM	Transverse Mercator map projection
UKF	Unscented Kalman Filter
UPS	Universal Polar Stereographic
U.S. DoD	United States Department of Defence
UTM	Universal Transverse Mercator
VV	Vägverket (Swedish National Road Administration)
WGS 84	World Geodetic System 1984

Chapter 1

Introduction

Advanced driver assistance systems like drowsiness detection can obtain information about the position of a vehicle determined from a lane position monitoring system. Volvo Technology Corporation (VTEC) develops a wide range of products of advanced driver assistance systems and an accurate positioning system is needed as input to a drowsiness detection system. This thesis was performed at VTEC from October 2010 to April 2011 and was a part of the Drowsi project. This thesis presents a positioning system, using camera information, Dead Reckoning (DR) sensors, Global Positioning System (GPS) and map data. This chapter will give a brief description about the background, problem specification, objectives and thesis outline.

1.1 Background

Today active safety is a growing area of research within the automotive industry. Providers of driver assistance systems develop a wide range of products to make the driving easier and safer. Modern vehicles are equipped with driver assistance applications like planning and guidance functions, but also active safety systems that consider danger awareness, drowsiness detection, driver behavior, and physical features about the vehicle. A great challenge that these improved safety systems and also navigation systems have is to determine the position of a vehicle with high accuracy. Many navigation and safety systems demand accurate positioning and mapping of the vehicle within the lane. Modern navigation systems commonly use Global Navigation Satellite Systems (GNSS), like GPS. The satellite coverage is not always ideal in urban areas because the GPS receiver can suffer from problems with e.g. signal masking, tunnels, multipath reflections and high buildings [1]. Signal masking occurs when the GPS receiver can not match at least four satellites to estimate a position [2]. Under these circumstances the GPS is normally improved with DR sensors in order to maintain accurate vehicle positioning. Such DR sensors in modern vehicles can be inertial sensors in for example anti-skid systems, gyroscopes measuring yaw rate of the ego vehicle, accelerometers measuring the longitudinal and lateral acceleration of the vehicle and odometric e.g. wheel-speed

sensors in Anti-Lock Braking System (ABS) accessible through a data bus, such as Controller Area Network (CAN). External sensors like cameras, Radio Detection And Ranging (RADAR) and Light Detection and Ranging (LIDAR) can also give useful information in order to determine the position of the vehicle in the lane. Since navigable maps, provided by for example NavTeQ [3] and TeleAtlas [4], store geographical information about the road network, navigable road maps can be utilized to determine the correlation between the road network and the position of the vehicle. Map data from navigable maps added to a positioning system can increase the accuracy of the position of the vehicle. Information from several different sensors are used to determine a more accurate position of the vehicle in the lane compared to using the sensors separately. This is called sensor fusion and it is also a big research area in the automotive industry.

1.2 Volvo Technology Corporation

This section is based on information from [5]. This thesis has been performed at the department of Human, Systems and Structures at VTEC in Gothenburg. VTEC has around 500 employees and is located at Lundbystrand and Chalmers Science Park in Gothenburg and also has establishments in Lyon, France, Greensboro and Hagerstown, USA, Bangalore, India and Ageo, Japan. VTEC is an innovation company with primary customers within the Volvo Group, but selected suppliers are also provided services. The main research and development areas at VTEC are transportation, telematics, internet applications, databases, ergonomics, electronics, combustion, mechanics, industrial hygiene and industrial processes and all development are done on contract basis. Human, Systems and Structures is a department that has a wide experience of research and development within the area of active safety systems and Human-Machine Interaction (HMI) integration. Some of the main research areas at the Intelligent Vehicle Technologies (IVT) group are development of Driving Assistance Systems e.g. lateral and longitudinal vehicle control, vehicle automation, vehicle-to-vehicle communication, collision avoidance, monitoring of driver drowsiness and distraction, etc..

1.3 Problem Specification and Goal

Camera information can be used in order to locate the position of the vehicle within the lane and therefore the camera can be considered as a lane positioning system. The goal of the thesis is to investigate if the robustness and availability of the lane positioning system (camera) can be increased by using additional sensor sources like map data and GPS. The goal of the thesis is also to investigate which performance this new lane positioning system has. In this thesis a camera, DR, GPS and map data are integrated with an extended Kalman filter (EKF) in order to estimate the position of a vehicle. Figure 1.1 shows an overview of the new lane positioning system. The idea with the lane positioning system is that it should give an estimate of where the vehicle is located within the lane, to a drowsiness detection system. The drowsiness detection system investigates the behaviour of

the driver to detect drowsiness. The drowsiness system was earlier developed in a project, which is named Drowsi, where among others Volvo Technology participated.

System overview

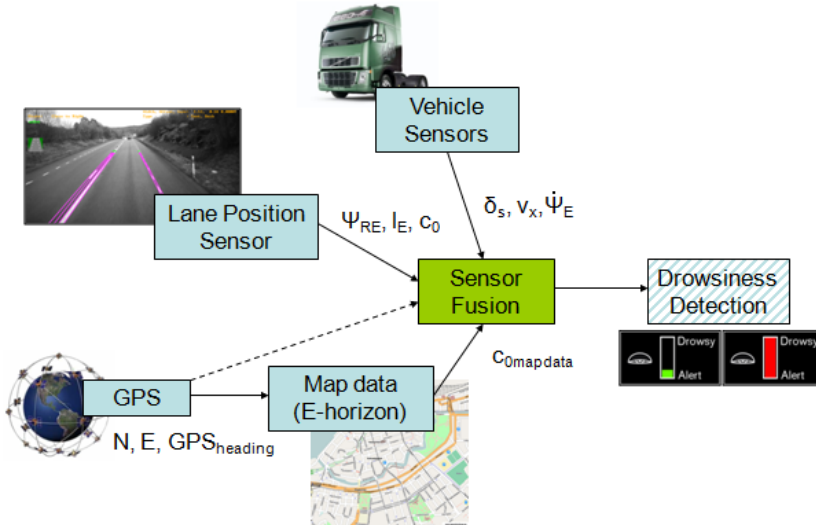


Figure 1.1. A system overview for the lane positioning system, [6]. The lane positioning system (system) consists of a lane position sensor (camera), vehicle sensors, map data and GPS, where the data/signals are sent to the sensor fusion algorithm. All signals are sent via different CAN buses, which is an electronic network used for communication between different components and systems in the vehicle. The signals from the camera are the relative angle between vehicle and road ψ_{RE} , the lateral displacement of the vehicle in lane l_E and the curvature at the ego vehicle c_0 . The signals that are coming from the vehicle sensors are steering wheel angle δ_s , the longitudinal velocity v_x and yaw rate $\dot{\psi}_E$. The signals that are coming from map data and GPS are the curvature from map data $c_{0mapdata}$ and $GPS_{heading}$, x and y position from GPS. The model of the system is a combined vehicle and road model. More descriptions about the system, model and signals can be found in chapters 7 and 8.

1.4 Contributions

The aim of this section is to give a brief summary of my contributions in this thesis work. My main contributions in this thesis are the following:

- The first part of the thesis was that the author did a pre-study what other authors have done in the area of investigating a lane positioning system and was presented as a literature study, see chapter 2. For instance, which

methods the authors are using and how the authors work is related to this thesis.

- The author collect data to be able to analyze the performance of the developed lane positioning system, see chapter 5. Vägverket (Swedish National Road Administration), here abbreviated SNRA has also collect data. These measured values from the collected data from the SNRA are considered as true and will be compared to the data that the author collected. The true values are then going to be a measure to see how good the model in this thesis is. To understand the different collected data, their behaviour and characteristic better two small parts from the route have been selected, see chapter 5.1.1 and 5.1.2 respectively.
- The author has developed a model for the lane positioning monitoring system, see figure 1.1. The model is an extended and modified model, based on a model called Single Track Model with Road Interaction (STMI) from the literature study, see chapter 2. The STMI model has been extended by adding measurements from additional sensor sources such as vehicle sensors, GPS and map data, see chapter 7.
- The author has extended the model from chapter 7 by integrating already known models such as GPS and DR model, constant velocity model, coordinated turn model to the extended model of the lane positioning monitoring system, see chapter 8. Measurements and estimations from additional sensor sources such as vehicle sensors, GPS and map data has been integrated into the extended model to match the lane positioning monitoring system.
- The states in the model in chapter 7 are estimated by an KF. The KF is based on the theory in chapter 6. The KF is implemented from scratch in Matlab by the author. The position of the vehicle in lane is estimated by the KF.
- The states in the extended model in chapter 8 are estimated by an EKF. The EKF is based on the theory in chapter 6. The EKF is implemented from scratch in Matlab by the author. The position of the vehicle in lane is estimated by the EKF.
- The author has translated C# code for the mathematical formulas and expressions for the transformations between coordinates in the WGS 84 frame and RT90 coordinates based on the theory from chapter 3.4 and implemented it into Matlab.
- Four different techniques described in chapter 9.1, 9.2, 9.3 and 9.4 have been developed by the author to be able to compare the estimated curvature from the EKF with data from SNRA. The fourth technique, see chapter 9.4, has also been divided by the author into three subtechniques.
- The author contributes an evaluation in order to investigate whether the robustness and availability of such a system increases, using additional sensor

sources like map data. Three cases have been tested, see chapter 9. Case A is when the curvature without map data is estimated by the EKF. Case B is when the curvature with map data is estimated by the EKF and Case C is when the curvature both with map data and with reliable camera data is estimated by the EKF. The author evaluated the solution offline using simulations and a signal that indicates if the LPS system has reliable camera data over a large sequence has been manually added to the system estimated by the EKF in the measurement update. There is a signal from the LPS system that indicates if the camera data is reliable and could be used for an online solution.

- The author presents in chapter 9, the results of the investigation, sensor fusions and enhancements techniques, tables and figures and Root Mean Square (RMS) values, described in chapter 9.5 is used to evaluate the performance of the lane position monitoring system.
- The author has made a summarization of conclusions from the results and evaluation of the lane positioning monitoring system presented in chapter 9. Some ideas for future work are also discussed by the author, see chapter 10.2.

1.5 Thesis Outline

In chapter 2 a literature study is presented of what other authors have done in the area of investigating a lane positioning system. For instance, which methods the authors are using and how the authors work is related to this thesis. Chapter 3 describes the theory of earth models, conversion between different coordinate frames, the theory of different coordinate frames and map projections. Chapter 4 presents different positioning techniques. In chapter 5 data collection and preprocessing needed for this thesis are discussed. In chapter 6 estimation theory is described. The model and the extended model for the lane positioning system are given in chapter 7 and chapter 8. Chapter 9 is a summary of the results and in chapter 10 conclusions from the results and some ideas for future work are discussed. Finally, in Appendix A, figures from the raw data are presented and Appendix B shows some figures from the results in chapter 9.

Chapter 2

Literature Study

The aim of this chapter is to give a brief introduction to what other authors have done in the area of investigating the performance of lane position monitoring systems and to investigate techniques for increasing the robustness and availability of such a system by using additional sensor sources like map data and GPS. The authors' works that have been studied in this literature study contains all variants of lane positioning systems, but it does not necessarily mean that it is the main subject of the authors' different works. The techniques for enhancing the accuracy of the positioning system and aspects the authors are looking at and how the different authors work (models, techniques, aspects) differ from each other. It is also of interest for this thesis to look at what other authors have done in the area of similar models for the ego vehicle and the using of lane and curvature information from a camera system.

2.1 Related Work with Positioning Systems using additional Sensor Sources

Digitally stored map information and a DR system are used by the author in [2] to produce a high performance vehicle positioning module. Signals to achieve accurate position are integrated from relative sensors like wheel speed sensors, accelerometers and gyroscopes with information stored from a digital map. The term relative sensors is used to describe sensors that measure the movements relative an absolute position [7]. The problem is formulated as a non-linear estimation problem to estimate the absolute position when the absolute heading is known. This solution uses Bayesian estimation. A grid based method that is referred to as the point-mass filter and a sequential Monte Carlo method has been investigated and evaluated. Simulation results show that by using this technique it is possible to obtain position estimates with accuracy comparable to the accuracy obtained if GPS is used. A positioning system based on the suggested method can both be used as a stand-alone solution or as a complement to other already existing systems. An extended model where the absolute heading angle is estimated by a

particle filter has also been considered. The aim in [2] is to use digitally stored map information and a DR system to obtain a more accurate vehicle position. The usage of map data in vehicle positioning and DR models in [2] are comparable with the ones in this work.

The authors in [8] use a DR system that receive information from low cost in-vehicle sensors like gyroscope and speedometers and a GPS receiver. The DR system and the GPS are integrated with an extended Kalman filter to obtain an estimate of the position of the vehicle. The system is able to give an estimated position in the horizontal plane with a relatively high update frequency and with the accuracy of the GPS receiver used when the evaluation of the positioning algorithm is implemented. In addition the system is also able to take care of GPS signal masking, chapter 1.1, for a certain period of time. An off-line map matching algorithm has also been implemented to give a more accurate position of the vehicle. The aim of [8] is to use DR and GPS to determine the position of a vehicle and to match the vehicle's position against a digital map. The DR approach for yaw rate and the transformation between WGS-84 and UTM coordinates and backwards in [8] are the same as in this thesis.

When it comes to appropriate models of positioning systems and the use of lane and curvature information [9] is also of interest. The author in [9] is concerned with automotive active safety, and the main theme is a safety function known as Emergency Lane Assist (ELA). ELA is a lane guidance system and such systems normally use a camera to monitor lane markings. This safety function requires a certain accuracy of the information from the sensors, in particular information about the road shape and the positions of surrounding objects. In addition, the ELA requires a robust threat assessment. In order to meet the higher accuracy requirements of the sensor information, several signal processing methods have been developed and evaluated. Each of the methods has been evaluated based on how much it improves the accuracy of the estimate from the sensor information and how it performs in relation to the requirement of the ELA. In addition, different threat assessment methods are studied. A common element in both signal processing and threat assessment is that they are based on driver behaviour models. This means that they speculate that drivers are more likely to behave in certain ways than others depending on the actual traffic situation that they are exposed to. Most of the studied methods are general, which means that there are possibilities to apply them in other safety systems, especially when the complete picture of the vehicle surroundings is considered. All methods studied in [9] have been evaluated using authentic sensor data from both actual and relevant traffic environments. The aim in [9] is to prevent accidents before they occur, which belongs to the area of active safety research. Appropriate driver behaviour models and the using of lane and curvature information comparable to this thesis can be found in [9]. The main methods employed in [9] are:

- An assessment method for new and potentially beneficial safety functions is included in the development of the new safety function Emergency Lane Assist (ELA). The ELA safety function has been evaluated in three ways. The

first evaluation is performed using simulations, the second by using artificial scenarios on a test track and the final evaluation uses authentic traffic data.

- Development and evaluation of different geometric models in an integrated filter for a combination of road shape estimation and target tracking.
- A demonstration of how to use change detection in order to detect lane changes of leading vehicles. This solution is then used to improve the lane shape estimation accuracy in the integrated filter.
- A demonstration of how a marginalized particle filter can be used in the integrated filter instead of an extended Kalman filter. The marginalized particle filter is based on a non-linear model.
- A method for obtaining true road geometry parameters from recorded sensor data, which can be used as a reference for filter tuning. An advantage is that this can be done without extra sensors or other hardware.
- A statistical threat assessment method based on vehicle dynamics and a driver behaviour model that is stochastic. A more accurate and longer prediction can be made using this method. This method also consider how the object interacts in the road scene.
- A dynamic vehicle model that can be used in curved, road-aligned coordinates. This means that the coordinate system used by the model is shaped according to the shape of the road. By using this model, the threat assessment can be carried out in the road-aligned coordinates immediately.

In the paper [10] the authors introduce a method for land-vehicle navigation systems. The main idea with this system is to fuse GPS and DR data. This is especially useful in urban areas where GPS outages can happen. The differential odometry of the vehicle is computed by the DR sensor. Fusing the road map database of a Geographical Information Systems (GIS) is also done by the authors algorithm. This is done with improving the positioning accuracy in mind. The digital road map is a measure of a set of node locations and road bearings in the model in [10]. The Mahalanobis metric is used to initialise this measurement equation. In order to allow a direct modelling of the map errors and uncertainties (embedded in the filter) this measurement equation is used. The available measurements are sequentially processed by the filter. This builds on a centralized fusion algorithm. In order to show the advantages for vehicle positioning of the suggested method the authors presents experimental results. These results are based on an urban transport network scenario where signals from the GPS are poor. The authors in

[10] solve the multisensor estimation problem by an extended Kalman filter (EKF) that fuses the GPS, odometer and road map data in order to get more accurate vehicle position in a similar way as this thesis solves the non-linear estimation problem. The vehicle locations in [10] are also given in UTM coordinates as in this thesis.

A data fusion strategy for the global localisation of car-like vehicles is presented in [11]. Raw GNSS measurements, DR sensors and road map data are used to build the system. Map information is used as a heading observation in a Kalman filter presented as a new method by the authors in [11]. The advantage of such a method when the GPS information is not available is shown by experimental results. A conservative localization strategy that is based on DR navigation is introduced by the authors in [11] when GPS outages happens. The map data and the GNSS measurements are not considered in cases when the consistency test are uncertain. The performance is better when only the available information is used consistently, as experimental results show. Map data, DR sensors and raw GPS data is fused in order to get global localization of car-like vehicles is the goal of this paper. The authors in paper [11] fuse GPS data, the DR sensors and the map data to get more accurate vehicle position in a similar way as this thesis solves the non-linear estimation problem. The ECEF frame is also used in [11] as in this thesis.

The author in [12] has modelled the ego vehicle with a Coordinated or Constant Turn Model. In order to construct this ego vehicle, the study uses a dynamic model called Single Track Model. This model includes a tire model which uses geometric relationships. Furthermore the model has an extension for modeling the road. Commonly this Single Track Model with Road Interaction is used for autonomous driving and lane keeping. The collection of external data is made possible through the use of three sensors. The first setup consists of a forward looking camera and radar. The second configuration also consists of a forward looking camera and radars, but with the difference that the radars are not only forward looking but can also point to the rear and side. The third set up is designed to give an axle height value by using internal or proprioceptive sensors. The study, which uses particle Filter (PF) and EKF variants, features sensor fusion in order to obtain better information than that which would be obtainable if separated sensors were used. Here [12] details how the motion of a tracked object is estimated and how properties of static objects such as road lines are calculated. In this study, the author discusses the problem of estimating the motion of an ego vehicle and its surroundings in order to improve the drivers' situational awareness. Appropriate models and the use of lane and curvature information for this thesis can be found in [12]. The model that has been chosen for this thesis study, is a modified and extended version of the model Single Track Model with Road Interaction featured in [12].

Chapter 3

Coordinate Systems and Geographical Positions

In this work an EKF is used to estimate the position of the vehicle in the lane. In order for the EKF to give an accurate estimate of the position of the vehicle all the signals from the different sensor sources have to be in the same coordinate system. The position of the vehicle from the positioning system is always described as a number of coordinates and a coordinate system is needed to determine where the vehicle is located. In order to model data from the different positioning techniques, described in chapter 4 it is also important to know which earth model and map projection that is used. This chapter will give a brief introduction to earth models, map projections and coordinate systems used in this thesis.

3.1 Models of the Earth

To describe a position on the surface of the earth an approximation of the earth is needed. Earth models that are used in this work are spheres, and the ellipsoids Bessel 1841 and WGS 84. A sphere with a fixed axis of rotation is the most used simple earth model in positioning and navigation systems, which frequently uses the surface of the earth as a reference [13].

To describe the shape of the earth a reference ellipsoid can be used as a simplification. A reference ellipsoid consists of a symmetric body around the rotational axis, in other words a rotational ellipsoid. Bessel 1841 is a reference ellipsoid. The semi-major axis in Bessel 1841 is approximately 6377 km and the polar radius is approximately 6356 km. In order to describe how flattened the earth model is the concept of flattening is introduced. The flattening f is defined as $f = \frac{a-b}{a}$, where a is equal to the semi-major axis and b is the polar radius. The inverse flattening is defined by $1/f$ and is in Bessel 1841 approximately 299.

The United States Department of Defense (U.S. DoD) has developed a more

complex earth model named the World Geodetic System 1984 (WGS 84), which is an international standard for navigation. In the earth model WGS 84, the equatorial radius is 6378 km, the polar radius is 6357 km, the ellipsoid's centre is at the earth's center of mass and the rotational axis is the earth's rotational axis. The inverse flattening is in WGS 84 approximately 298.

3.2 Cartesian, Geocentric and Geodetic Coordinates

Geocentric, geodetic and 3D Cartesian coordinate systems are used in positioning applications. For defining the coordinates of a point with geocentric coordinate system, shown in Figure 3.1, one can use the following scheme: define the mass centre of the earth as the origin and give the latitude (ϕ), longitude (λ) and distance from the origin to the point itself (r) [7].

To define a geodetic coordinate system, one needs to have a given ellipsoid and plane through the polar axis of the ellipsoid [7]. In Figure 3.2 a 3D cartesian coordinate system and a geodetic system are shown. The angle between the equatorial plane and the extension of the normal to the ellipsoid surface towards the interior of the earth is defined as the geodetic latitude (ϕ). Observe that the extension of the normal to the ellipsoidal earth model towards the interior of the earth generally will not intersect the centre of the earth according to the elliptic form of the earth model. The angle in the equatorial plane between the prime meridian and the orthogonal projection of the point of interest in the equatorial plane is defined as the geodetic longitude (λ). The distance between the point of interest and the ellipsoid, measured along the normal to the surface of the ellipsoid is defined as the geodetic height (d) [7]. The goal is to construct an ellipsoid that is as good approximation for the surface of the mean sea level as possible in order to be able to use the geodetic height as an approximation for height over the sea level. Note that for instance in air navigation the height over the surface of the earth is critical and therefore the geodetic height should be treated carefully.

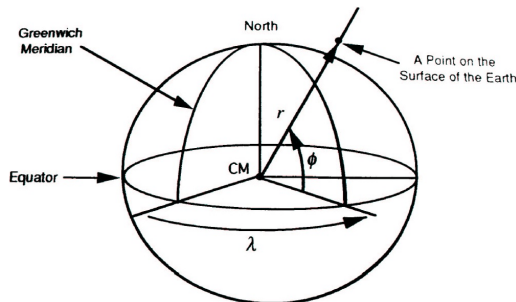


Figure 3.1. A geocentric coordinate system with latitude ϕ , longitude λ and the distance from the origin to the point itself r . CM is the mass centre of the earth [7], [8].

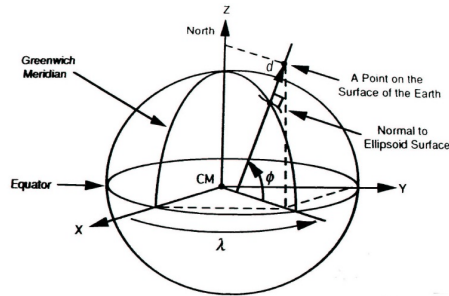


Figure 3.2. A geodetic coordinate system with latitude ϕ , longitude λ and the geodetic height d and a cartesian coordinate systems with coordinates X , Y and Z . The mass centre of the earth is abbreviated with CM [7], [8].

Geodetic coordinates are often used. This is because in positioning and navigation 3D cartesian coordinates are not appropriate and as an example if moving north a certain distance, except at the equator, it will not result in an increase only in the Z value (assuming Z defined as pointing north). For geodetic coordinates the same movement always give an increase only in latitude. When geodetic coordinates are used in positioning systems they cause some problems. Formulas for 2D cartesian coordinates are more straightforward to use than corresponding mathematical formulas for calculating a distance from geodetic coordinates. The geodetic latitude and longitude coordinates are often transformed to 2D cartesian coordinates [7], this is to avoid problems. In this thesis if nothing else is said, a 2D map is always considered when a map is referred. In this case map projections are the transformation between geodetic and 2D cartesian coordinates and what type of 2D projection used depends on what is to be modelled. To be able to transition from geodetic coordinates to flat two-dimensional coordinates one applies a map projection, see 3.3.

3.3 Map Projections

A map projection projects the surface of the ellipsoid on a plane and can be considered as the link between the reference ellipsoid and the map. This section describes two sorts of map projections: conformal and equivalent projection. The first of the two map projections is conformal and in this projection all angles are preserved. The angles on the surface of the earth are equal to the angles on the map. The second map projection is equivalent projection. In this projection when comparing any area on the map and the corresponding area on earth a constant ratio is achieved. Projections can not be both conformal and equivalent [7]. A projection is exact when a map projection is used to transform one type of coordinates to another type of coordinates without losing data. Regardless of which type of projection that is used, when approximating the 3D spherical earth with the 2D representation, it is impossible to be exact in every aspect.

A 2D projection of the earth is used to make an approximation. The errors in this approximation are negligible for common map users. Many projections have been made to approximate a certain local area accurately. However, if these projections are used on other areas they will lead to poor or even invalid projections, which means they are not very useful for worldwide applications unlike the conformal Universal Transverse Mercator (UTM) projection. A GPS can be integrated with a DR system, described in section 4.2, which often outputs its data in UTM coordinates. In this case one option is to transform WGS 84 coordinates to UTM coordinates (this transformation is called the UTM projection, not to be confused with UTM coordinates).

It is possible to divide the surface of the ellipsoid earth model. UTM divides the earth model into 60 zones, each 6 degrees wide in longitude. A zone reaches from 80 degrees S to 84 degrees N and the central meridian is also in the centre of the zone. The N axis is defined in north direction and the E axis is defined in the east direction. 2D cartesian coordinates are used. For the areas north of the latitude 84 degrees north, and south of 80 degrees south, a Universal Polar Stereographic (UPS) projection has been used. Since the data collection for this thesis did not take place in these areas UPS will not be further described. The UTM coordinates are given in metres and are referred to as northing and easting [7]. The point where the central meridian intersects the equator is the origin of each zone. A problem occurs if all points west of the central meridian in the zone either have to be given negative values or assigned with a direction. This is the case if the origin is assigned with the value of zero. In order to counter this the central meridian in each zone is given a false easting of 500 000 m. Because this values will be lower than 500 000 to the points west of central meridian. If referring to a position in the southern hemisphere, the equator is given a false northing of 10 000 000 m. Similarly, if referring to a position on the northern hemisphere a false northing of 0 can be given [14]. This is because all points in the southern hemisphere have to be negative or assigned with a south direction when the equator would be given the northing value 0. The UTM projection is easy to use for a positioning system design working in one zone and transitions between different zones are more difficult to handle. The UTM projection is a worldwide projection.

This section is based on [15]. The Swedish grid (in Swedish RT90, Rikets Nät) is a newer modified version of the coordinate system RT38 from 1938. RT90 uses a Gauss conformal projection which preserves the angles and the chosen central meridian in the longitudinal direction, and it is used for Swedish government maps. Synonyms for Gauss conformal projection are Gauss-Krüger (GK) and transverse Mercator map projection (TM). Starting from the central meridian to the actual system of projection the x -coordinates are calculated positive north and the y -coordinates positive east. In order to avoid negative y -coordinates an addition of 1500 km has been made. Now the central meridian is defined in relation to zero central meridian in Greenwich, but from the beginning the central meridian

is defined as 2.5 gon (1 gon = 0.9 degrees) west of the Stockholm Observatory. SWEREF 99 is a three-dimensional reference system. SWEREF99 has its origin in the mass centre of the earth. In the future SWEREF99 is going to replace RT90.

3.4 Coordinate Frames

A coordinate system can specify the location of a point using a vector from an origin to the point itself. Some coordinate frames are being used to design the positioning system in this thesis. There are several frames; the earth-centred, earth-fixed (ECEF) coordinate frame rotates with the earth and has the X-axis towards the Greenwich meridian. For describing the location of the point in an ECEF frame the three-dimensional (3D) cartesian coordinates and geodetic coordinates are useful. In section 3.2 more information about different coordinates can be found. The second earth frame, WGS 84 frame, is also earth-fixed and earth-centred. The WGS 84 ellipsoidal earth model and geodetic coordinates are used. The WGS 84 frame is actually an example of an ECEF frame and has its prime meridian through Greenwich. The third frame, NEZ frame (NEZ after its axes North East Height), has its origin in the vehicle typically centre of sensor cluster or mass centre of the vehicle. In the NEZ frame, the N-axis always points north, E-axis always points east and Z-axis points up from the centre of the earth. Finally, the last frame in this thesis, the Body frame, has the same origin as the NEZ coordinate frame and the X-axis is in the direction of the vehicle, the Z-axis is through the roof of the vehicle and the Y-axis forms the right hand orthogonal coordinate frame.

This work uses mathematical formulas and expressions for the transformations between coordinates in the WGS 84 frame and UTM coordinates described in [8]. The mathematical formulas and expressions for the transformations between coordinates in the WGS 84 frame and RT90 coordinates is from [15], [16] and [17].

Chapter 4

Positioning Techniques Related to This Thesis

The three main approaches to determine the position of the vehicle today are stand-alone, satellite based and terrestrial radio based. A stand-alone device is self-contained and does not require any other devices to function. A satellite navigation system uses satellites to determine the position of the vehicle. Terrestrial radio based system for positioning use base stations and antenna system for mobile phones, two-way radios, microwave applications and Personal Communication Systems (PCS) to broadcast signals to the vehicle. Positioning in mobile radio systems can be found in [18] and is an example of a terrestrial radio based approach used for positioning. This thesis will present a combination of two of these approaches. These two approaches are camera and DR, which are stand-alone approaches and GPS, which is a satellite based positioning system. To set up a DR algorithm, speed and direction of travel are used and measured from in-vehicle sensors. If a DR model is combined with map data and GPS, a more accurate system can be obtained and certain drawbacks can be avoided, compared to using the two models separately [19].

4.1 Camera

A camera can be used as a vehicle positioning system in the lane. Maps and 3D models can be automatically designed from camera data. An image sensor alone can be used for pose, i.e. position and direction, estimation and structure reconstruction. This is called Structure from Motion (SfM), [20]. SfM is a cost-efficient approach when augmented imagery application, which is generated by adding virtual objects into real images, is created. SfM is cost-efficient since it requires no additional hardware. A single camera SfM matches image features between consecutive image frames and, based on a geometric camera model, estimate the camera poses and 3D positions of the observed features. This is the most common approach for single camera SfM. SfM fails when image features cannot be

matched robustly between consecutive frames. This happens when image information is poor, which is the main drawback with SfM. Using Bundle Adjustment (BA) accuracy can be improved by optimizing an estimate numerically. An initial estimate that is accurate enough to converge is required for BA in order to improve accuracy and robustness, as shown in e.g. [21] and [22]. A single track vehicle motion model can be included in a BA framework [23]. Accuracy of visual BA can be combined with vehicle motion models and standard in-vehicle sensor data (like wheel speeds, yaw rate and steering wheel angle). The system creates an accurate and robust pose estimate for a camera. BA is often computationally demanding, which is not the case for the camera mentioned in chapter 1.3 where the outputs of the camera is lane positioning data. This work uses the signals relative angle between vehicle and road, lateral displacement of the vehicle in lane, curvature at the ego vehicle from a LPS system in order to determine the position of the vehicle in lane. The data from LPS system will be further described in chapter 5.

4.2 Dead Reckoning

A DR system calculates the position of the vehicle at any time instance, if the starting location and all previous displacements are known. DR systems calculate the travelled distance and the direction of travel. Inertial Navigation System (INS) is an example of a DR system, and it calculates the position of a vehicle from its acceleration and angular velocities. In this thesis another DR approach is considered where the position of the vehicle and attitude¹ are calculated from the longitudinal velocity v_x and the yaw angle of the ego vehicle ψ_E . The yaw rate and attitude are supposed to be constant, while the longitudinal velocity is changing during a sample period. This approach of DR system has the following equations:

$$N_{(t+1)} = N_{(t)} + T * v_{(x)} * \cos\psi_{E(t)} \quad (4.1)$$

$$E_{(t+1)} = E_{(t)} + T * v_{(x)} * \sin\psi_{E(t)} \quad (4.2)$$

$$\psi_{E(t+1)} = \psi_{E(t)} + T * \dot{\psi}_{E(t)}, \quad (4.3)$$

where N and E are the north, east position coordinates. T is the sample time and ψ_E is the yaw angle, which is defined as in Figure 4.1. DR systems have the advantage that they can be run with a high sample frequency compared to the GPS. Drawbacks with DR systems are errors in position and attitude that comes from sensor inaccuracies and the assumption of constant yaw rate, attitude and the longitudinal velocity is changing over a sample period. The calculated position is less accurate over time because errors in position and attitude tend to accumulate as the vehicle continues to travel.

¹The attitude is the relation between the body frame and the NEZ frame and can be described with three angles, namely the yaw angle, the pitch angle and the roll angle [24]. In this thesis only the yaw angle is referred to as the attitude.

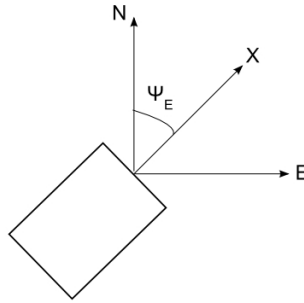


Figure 4.1. The definition of the yaw angle ψ_E

4.3 GPS

The GPS is a global satellite-based radio navigation system developed by the United States Department of Defense (U.S DoD) originally for military purposes but is nowadays also accessible for civilians. The GPS consists of at least 24 satellites arranged in six orbital planes. Each satellite carries a high precision atomic clock and broadcasts encoded messages at regular and known time instants. Each message includes an identification number and the location of the satellite. A receiver on the ground decodes the signal and uses the signal propagation time to calculate a pseudorange. In order to determine its position, the receiver needs to know the pseudorange to the satellites and their locations. Simultaneous observation of at least four unique satellites permits determination of the 3D coordinates of the receiver. The coordinates can be calculated in, for example, a WGS-84 frame or an ECEF-frame [5]. Certain drawbacks with the GPS receivers is low sample frequency, low resolution, low accuracy, multipath, loss of GPS position through urban canyons or road tunnels. The multipath effect is due to reflection of GPS signals on blocking objects and mainly appears in the surroundings of large buildings or other elevations. The reflected signal is detected later by the GPS receiver than the direct signal. The consequence is an error in the range of a few meter of the estimated GPS position. One advantage of GPS receivers is that they do not suffer from error growth, which occurs for DR systems. DR systems run with high sample frequency and they do not have the risk for signal masking, chapter 1.1, which is an another drawback with GPS.

Chapter 5

Data Collection and Preprocessing

This chapter describes the data collection and preprocessing of the signals before the signals are evaluated. The purpose of this chapter is also to give a better understanding of the signal's behaviour and characteristics.

5.1 Data Collection

One of Volvo's test trucks was used to collect data. The test vehicle started to collect data near Lundbyvassen in Gothenburg to Kullamotet near Bollebygd and back again to Volvo Technology's garage at Götavergsgatan see figure 5.1. The route took one hour five minutes and 54 seconds to drive.

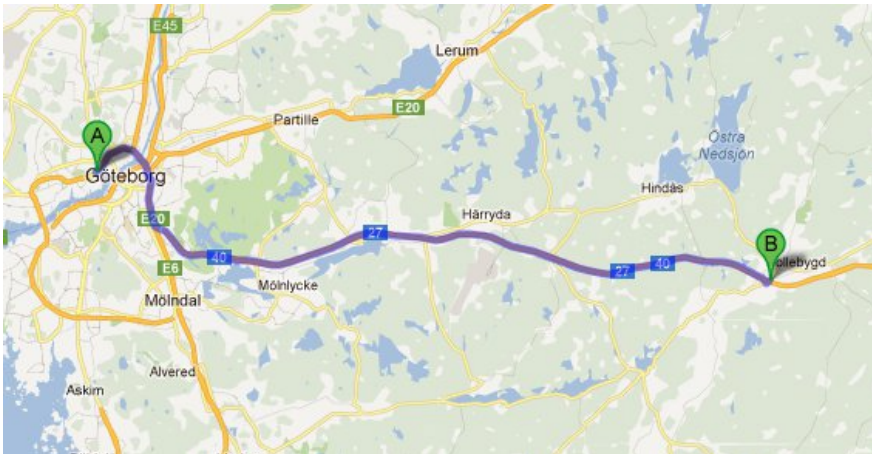


Figure 5.1. The route from Lundbyvassen in Gothenburg to Kullamotet near Bollebygd

The test vehicle was equipped with camera, gyroscope and a GPS receiver. All signals were sent from different Controller Area Network (CAN) buses, which is an electronic network used for information communication between different components and systems in the vehicle. An industrial PC and Vector CANape were used to collect and store the data. The Vector CANape is a data collection program, installed on a computer.

There were three different kinds of data from the test vehicle, namely data from LPS system, data from vehicle sensors and data from GPS. This issue will be discussed further in this chapter together with the preprocessing of the collected data.

To understand the different data from the LPS system, data from vehicle sensors, data from GPS their behaviour and characteristic better two small parts from the route have been selected named Data sequence 1 and Data sequence 2. Data sequence 1 and Data sequence 2 are discussed in chapter 5.1.1 and 5.1.2.

5.1.1 Data Sequence 1

Data sequence 1 is a road stretch with curves without any disturbance except that the test vehicle passed a connecting road at the time 532 seconds and an overtaking car crossed the center line of the lane at the time 582 seconds. The different signals from the LPS system, from the vehicle sensors, from the GPS figures of Data sequence 1 are listed in table 5.2, 5.4 and 5.6.

5.1.2 Data Sequence 2

It is also important to know how the data from the LPS system, data from the vehicle sensors, data from the GPS behaves and their characteristics under disturbance. The disturbance is caused by overtaking cars of the test vehicle at the time 665 seconds, 704 seconds, 714 seconds, turning road at the time 665 seconds, the test vehicle is going under a bridge at the time 680 seconds, connected road at the time 698 seconds. The connected road can explain why the LPS system lost connection for a while around the time 694 seconds because it do not know which lines of the two lanes it should be tracking. In table 5.2, 5.4 and 5.6 figures of data sequence 2 for the different signals from the LPS system, from the vehicle sensors and from the GPS are listed.

5.1.3 Data from the LPS System

This section is based on information from [25]. The Lane Position Sensor (LPS) system is a closed system. An image processing system helps the LPS system to monitor the position of the vehicle in lane. Visible lane markings are used, also curbs and road boundaries may in some cases be detected by the LPS system. This happens when the road has no visible lane markings on the outside. The LPS system determines the most probable lane from a combination of all detected lane markings. Other functionalities of the LPS system is that the measurement is stabilized from the tracked lane markings that are found, but the system also

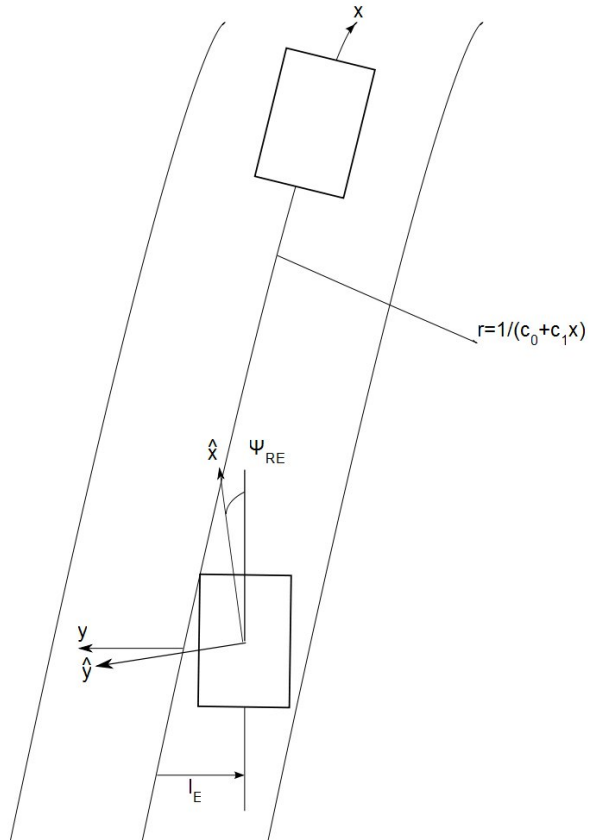


Figure 5.2. The relation between the signals that are coming from the LPS system and the vehicle and the road

seperates changes in road layout from ego movements and the predicted detection range. The LPS system includes a camera, which is mounted inside the vehicle. The camera tracks the white dashed lines in the lane. Figure 5.2 shows how the signals that are coming from the LPS system are related to the vehicle and the road. The signals from the LPS system will be further discussed in chapter 7.1. For how they are decided see chapter 5.2.1. The sampling frequencies of the data from the LPS system are proprietary information and will not be mentioned in this thesis. The relative angle between vehicle and road ψ_{RE} has the unit in radians, the lateral displacement of the vehicle in lane l_E has the unit metre and the curvature at the ego vehicle c_0 has the unit m^{-1} . In table 5.1 information from the LPS system are listed. Since all three variables in the table 5.1 are determined from the LPS system, the measurement error will be dependent. The relative angle is given between -45 and 45 degrees. The relative angle of the data from the LPS system is given with a certain resolution. This explains the quantified effects and that the relative angle is discrete in levels in figure A.7, A.8 for Data sequence 1 and in figure A.21, A.22 for Data sequence 2. However the resolution is proprietary information and can not be disclosed. The curvature is defined between $-1/250 m^{-1}$ and $+1/250 m^{-1}$. Similary to the relative angle of the data from the LPS system, the curvature of the data from the LPS system is given with a certain resolution. This explains the quantified effects and that the curvature is discrete in levels in figure A.10, A.11 for Data sequence 1 and in figure A.24, A.25 for Data sequence 2. However the resolution is proprietary information and can not be disclosed.

Table 5.1. Information from LPS system

Signal	Symbol	Unit
The relative angle between vehicle and road	ψ_{RE}	rad
The lateral displacement of the vehicle in lane	l_E	m
The curvature at the ego vehicle	c_0	m^{-1}

Table 5.2. Figures from data from left (l) and right (r) lane marker of the LPS system

Signal	Data sequence 1	Data sequence 2
The relative angle between vehicle and road	l:A.7, r:A.8	l:A.21, r:A.22
The lateral displacement of the vehicle in lane	A.9	A.23
The curvature at the ego vehicle	l:A.10, r:A.11	l:A.24, r:A.25

5.1.4 Data from Vehicle Sensors

The sampling frequencies of the data from the vehicle sensors are proprietary information and will not be mentioned in this thesis. The signals that come from the vehicle's sensors are steering wheel angle δ_s has the unit in radians,

the longitudinal velocity v_x has the unit metre per second and yaw rate $\dot{\psi}_E$ which is measured by a gyro and has the unit radians per second. In table 5.3 information from the vehicle sensors are listed.

Table 5.3. Information from vehicle sensors

Signal	Symbol	Unit
Steering wheel angle	δ_s	rad
Longitudinal velocity	v_x	m/s
Yaw rate	$\dot{\psi}_E$	rad/s

Table 5.4. Figures from data from vehicle sensors

Signal	Data sequence 1	Data sequence 2
Steering wheel angle	A.12	A.26
Longitudinal velocity	A.13	A.27
Yaw rate	A.14	A.28

5.1.5 Data from the GPS

The GPS receiver that has been used is a Garmin GPS 18 [26] receiver and the signals that are coming from map data and GPS are the curvature from map data $c_{0mapdata}$ and has the unit m^{-1} , $GPS_{heading}$ and has the unit in degrees, x and y position which gives the position in longitude and latitude and have the unit in degrees from GPS are all sampled with 1 Hz. How data from the GPS is decided is further discussed in chapter 5.2.3. In table 5.5 information from the data from GPS are listed.

Table 5.5. Data from GPS

Signal	Symbol	Frequency	Unit
X-coordinate of GPS	x_{GPS}	1 Hz	degree
Y-coordinate of GPS	y_{GPS}	1 Hz	degree
GPS heading	$GPS_{heading}$	1 Hz	degree
Curvature from map data	$c_{0mapdata}$	1 Hz	m^{-1}

Table 5.6. Figures from data from GPS in WGS 84 (l) and in RT90 (r)

Signal	Data sequence 1	Data sequence 2
X-coordinate of GPS	l:A.15, r:A.16	l:A.29, r:A.30
Y-coordinate of GPS	l:A.17, r:A.18	l:A.31, r:A.32
GPS heading	A.19	A.33
The curvature from map data	A.20	A.34

5.1.6 Data from the Swedish National Road Administration

Vägverket (Swedish National Road Administration), here abbreviated SNRA, has driven part of this route and measured it with laser scanners. This route is located on the countryside outside Gothenburg and was driven from Öis gården to Kullamotet near Bollebygd see figure 5.3. The collected data from the SNRA were given as a csv-file and were loaded into Matlab. The collected data from the SNRA that is useful for this thesis includes distance, velocity, x-, y-position and curvature defined positive for left turn. These measured values are considered as true and will be compared to the data that were collected from Volvo's truck. The true values are then going to be a measure to see how good the model in this thesis is.

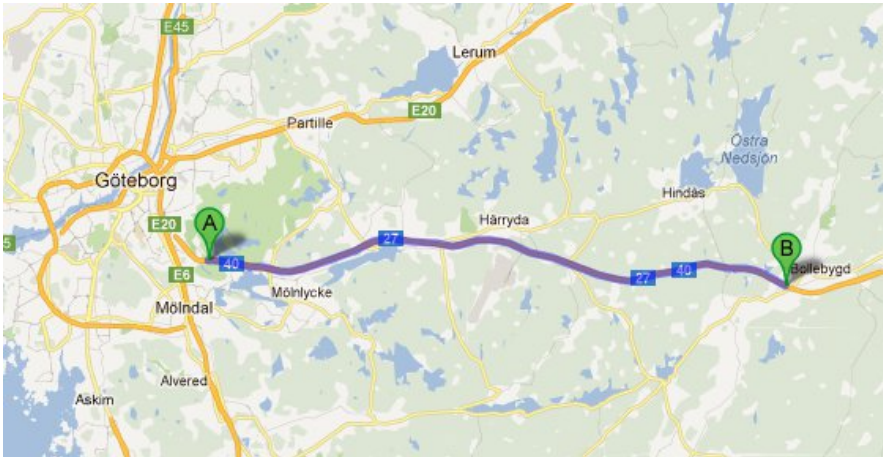


Figure 5.3. The Swedish National Road Administration's route from Öis gården to Kullamotet near Bollebygd

The collected data from the SNRA is sampled every metre. The curvature has the unit 10000 per metre and is defined positive for left turn. In table 5.7 information from the data from the vehicle sensor's are listed.

Table 5.7. Data from the Swedish National Road Administration.

Signal	Symbol	Unit	Figure
Distance	s_v	metre	A.2
X-coordinate of GPS	x_{GPS}	degree	A.3
Y-coordinate of GPS	y_{GPS}	degree	A.4
Curvature	c_{0Lv}	10000/m	A.5
Longitudinal velocity	v_{xv}	km/h	A.6

5.2 Preprocessing

The inputs and measurement signals from the vehicle sensors (yaw rate, velocity, steering wheel angle), LPS system (camera), map data and GPS are preprocessed before the signals are estimated by the EKF. E.g mean value calculations and some signals are linear interpolated in order to get the signals in the same time basis are some examples of preprocessing.

5.2.1 Data from the LPS system

Notice from the figures listed in table 5.2 that the data from the LPS system is discrete in levels and have quantified effects that depends on internal signal processing have been made in the LPS system [25]. The relative angle between vehicle and road ψ_{RE} and the curvature at the ego vehicle c_0 from the LPS system is measured both on the left side and right side on the vehicle. Separately linear interpolation has been done to have relative angle between vehicle and road respectively curvature left and right in the same time basis. Mean value calculations have been made also to give relative angle between vehicle and road ψ_{RE} and the curvature at the ego vehicle c_0 from the LPS system in the middle. The curvature at the ego vehicle c_0 from the LPS system in the middle is defined positive right in the figures in this thesis.

5.2.2 Data from the Vehicle Sensors

To obtain the front wheel angle δ_f , the steering wheel angle δ_s is divided by 17, see chapter 7.1. To obtain the estimated yaw rate $\dot{\psi}_E$, described in chapter 7.1, the front wheel angle δ_f and the longitudinal velocity v_x were linearly interpolated to get the measurements in the same time basis. Since longitudinal velocity v_x was measured at a lower rate than δ_f , its time basis was chosen. The estimated yaw rate $\dot{\psi}_E$ was then calculated as front wheel angle δ_f multiplied by the longitudinal velocity v_x and then divided by the wheel base on the vehicle l_b .

5.2.3 Data from the GPS

The GPS uses the reference system WGS84, which gives the position in longitude and latitude. The signals from GPS are converted to x- and y-coordinates in RT90,

see chapter 3.4. This transformation has been implemented in Matlab. After data collection x-, y-position and time from GPS is sent into Volvo's map data program [27], [28]. The map data program take out road attributes from a given map and gives out map data matched with x-, y-position and time. The map data program outputs a set of road attributes but since this thesis was interested in sensor fusion the curvature from map data with the curvature from LPS system only the curve radius were selected of the road attributes. Since the curvature from map data is noisy the signal has been low pass filtered. The low pass filter that has been used is a sixth order Butterworth filter with the cutoff frequency of 0.25 Hz.

5.2.4 Data from the Swedish National Road Administration

The curvature from the SNRA is divided by 10000 to obtain the unit m^{-1} and the longitudinal velocity from the Swedish National SNRA is divided by 3.6 to obtain the unit m/s see chapter 5.1.6. Since the curvature from the SNRA included white noise the signal has been low pass filtered. The low pass filter that has been used is a sixth order Butterworth filter with the cutoff frequency of 0.25 Hz. The white noise can be due to the SNRA measure equipment or other vibrations in the vehicle (i.e. not input related to curvature).

Chapter 6

Theory

The purpose of this chapter is to give a brief introduction to the Kalman filter and the extended Kalman filter theory. There are many books about this subject and this thesis uses similar notations and equations as in [29]. More about Kalman filter and extended Kalman filter theory can be found in [30].

6.1 The Linear State Space Model

The states in a linear state space model are

$$x_{k+1} = F_k x_k + G_{u,k} u_k + G_{w,k} w_k, \quad (6.1)$$

$$y_k = H_k x_k + D_k u_k + v_k, \quad (6.2)$$

where x_k is the state vector and y_k is the output of the system. F_k is the system matrix, $G_{u,k}$ is the system input matrix, $G_{w,k}$ is the process noise matrix, H_k is the measurement matrix, D_k is the measurement input matrix.

The process noise w_k and the measurement noise v_k are Gaussian noise with the following properties:

$$E(w_k) = 0, \quad (6.3)$$

$$E(v_k) = 0, \quad (6.4)$$

where $E(x)$ is the expectation of x .

$$COV(w_k) = Q_k, \quad (6.5)$$

$$COV(v_k) = R_k. \quad (6.6)$$

Q_k is the covariance matrix of the process noise and R_k covariance matrix of the measurement noise.

6.2 The Kalman Filter

The states in a linear state space model can be estimated by the Kalman filter (KF). The KF is initialized with

$$E(x_0) = \hat{x}_{1|0}, \quad (6.7)$$

$$COV(x_0) = P_{1|0}. \quad (6.8)$$

The double time index $k|m$ means time k given measurements up to time m . P is the covariance matrix of the state estimation error. Equation (6.1) implies (without any observations) that the initial state (6.7) and covariance (6.8) are propagated as

$$\hat{x}_{k|0} = F_k \hat{x}_{k-1|0}, \quad (6.9)$$

$$P_{k|0} = F_k P_{k-1|0} F_k^T + G_k Q_k G_k^T. \quad (6.10)$$

Algorithm 6.1 Consider a model described by $p(y|\theta)$, a conditional probability density function (PDF) where y is an observation due to a parameter θ . A good estimator $\hat{\theta}$ is sought. To map α , the observations to an estimate, an estimator $\hat{\theta} = \alpha(y)$ is introduced. The mean square error (MSE) is denoted as

$$MSE(\theta) = E((\theta^\circ - \hat{\theta})^2) = E((\hat{\theta} - E(\hat{\theta}))^2) + (\theta^\circ - E(\hat{\theta}))^2,$$

where θ° is the true parameter. Let introduce the best linear unbiased estimator (BLUE). The linear functions $\hat{\theta} = \alpha(y) = Ly$ that minimizes the MSE are bounded by the BLUE as well as the estimator to be unbiased. In order to get the best linear unbiased filter for the linear model (6.1), the following recursions are used and initialized with $\hat{x}_{1|0} = E(x_0)$ and $P_{1|0} = COV(x_0)$:

1. Measurement update.

The observation up to time k have been used to form the estimate $\hat{x}_{k|k}$ of the state x_k

$$\hat{x}_{k|k} = \hat{x}_{k|k-1} + K_k \epsilon_k, \quad (6.11)$$

$$P_{k|k} = P_{k|k-1} - K_k H_k P_{k|k-1} = P_{k|k-1} - K_k S_k K_k^T. \quad (6.12)$$

2. Time update.

$$\hat{x}_{k+1|k} = F_k \hat{x}_{k|k} + G_{u,k} u_k, \quad (6.13)$$

$$P_{k+1|k} = F_k P_{k|k} F_k^T + G_{w,k} Q_k G_{w,k}^T \quad (6.14)$$

Where the innovation is defined as

$$\epsilon_k = y_k - H_k \hat{x}_{k|k-1} - D_k u_k, \quad (6.15)$$

for the innovation covariance is given by

$$S_k = H_k P_{k|k-1} H_k^T + R_k, \tag{6.16}$$

and Kalman gain is defined as

$$K_k = P_{k|k-1} H_k^T (H_k P_{k|k-1} H_k^T + R_k)^{-1}. \tag{6.17}$$

The measurement update can then be written

$$\hat{x}_{k|k} = \hat{x}_{k|k-1} + K_k \epsilon_k, \tag{6.18}$$

$$P_{k|k} = P_{k|k-1} - K_k H_k P_{k|k-1} = P_{k|k-1} - K_k S_k K_k^T. \tag{6.19}$$

Time update (prediction) \longrightarrow Measurement Update (correction)

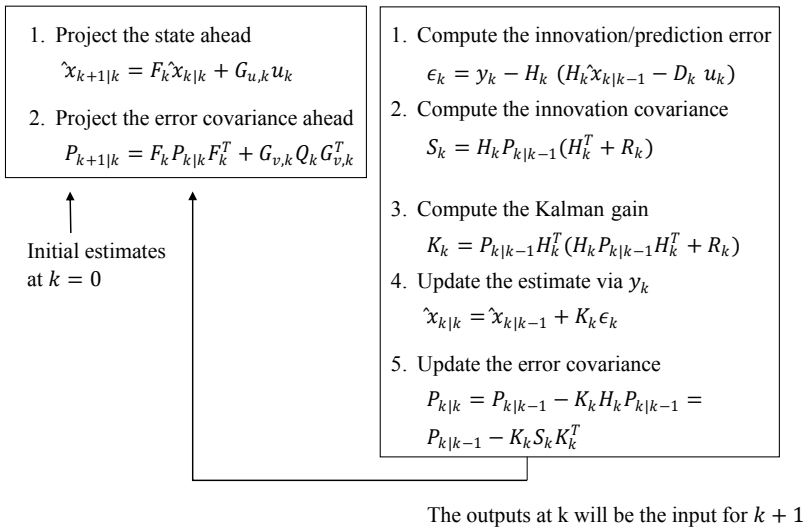


Figure 6.1. Kalman filter: Overview of the calculation.

6.3 Overview of the Calculations in the KF

The KF algorithm is recursive, which means the optimal estimate of the current state can be calculated from the estimated state of the previous time step and the current measurement. The KF algorithm can be divided into two parts; time update (prediction) and measurement update (correction). An overview of the calculations in the KF can be found in figure 6.1. First the KF are initialized with $E(x_0) = \hat{x}_{1|0}$ and $COV(x_0) = P_{1|0}$. In the time update, the KF estimates the current state from the previous state. This can be applied when no new

information have been obtained in the KF. See the equation in step 1 in figure 6.1. The first term in the equation in step 2 indicates how the uncertainty in the estimate is propagated to the next point. The second term indicates how much uncertainty increases because of the noise w_k in the equation (6.1). The next step is to calculate the measurement obtained at the time k i.e. y_k , should be weighted in the time update equations. In the measurement update, the prediction error/innovation ϵ_k is calculated and can be interpreted as the genuinely new information in the measurement y_k . The new genuine information is the part of the measurements that can not be explain of the estimates of the state i.e. $\epsilon_k = y_k - \hat{y}_{k|k-1}$. In step 2 in figure 6.1 the innovation covariance S_k is computed. In step 3 in figure the Kalman gain K_k is computed. K_k is a function of the relative certainty of the measurements $P_{k|k-1}$ and the measurements y_k of the current state estimate $\hat{x}_{k|k}$. A high Kalman gain means that the KF places more weight on the measurements i.e., the filter rely more on the measurements. A low Kalman gain means that the KF rely more on the model predictions in order to smooth out noise but deacrising the responsiveness. S_k together with K_k represents the second term in equation 5 in figure 6.1 and indicates how much uncertainty $P_{k|k-1}$ is reduced by weighting the data into the new measurement y_k according to equation 4. The outputs at k will be the input for $k + 1$ and then the algorithm begins again.

6.4 The Nonlinear State Space Model and EKF

The states in a nonlinear state space model with additive Gaussian noise

$$x_{k+1} = f(x_k, u_k) + w_k \quad (6.20)$$

$$y_k = h(x_k, u_k) + v_k. \quad (6.21)$$

The extended Kalman filter (EKF) estimates the states in a nonlinear state space model with additive Gaussian noise. The nonlinear filter recursion has one measurement update (similar to the Kalman filter in the linear case). This is provided that $\hat{x}_{k|k}$, $P_{k|k}$ and a time update yielding are present. First order Taylor expansion of a nonlinear function $z=g(x)$ is made around \hat{x} ,

$$z = g(x) \approx g(\hat{x}) + g'(\hat{x})(x - \hat{x}), \quad (6.22)$$

where $x \sim \mathfrak{R}^{n_x}$ and (initially for notational convenience) $z \sim \mathfrak{R}^1$. $g'(\hat{x})$ denotes the Jacobian evaluated at \hat{x} and this can be related to a linear state space model by the Kalman filter.

Here detailed recursions for the extended Kalman filter (EKF) will be given. The function $h(x, u, 0)$ is written more compactly $h(x)$, and similiary $f(x) = f(x, u, 0)$. The transformation approximation gives Riccatti-based EKF. The matrices

$(h'_x(\hat{x}))_{ij} = \frac{\delta h_i(x)}{\delta x_j} |_{x=\hat{x}}$ and $(f'_x(\hat{x}))_{ij} = \frac{\delta h_i(x)}{\delta x_j} |_{x=\hat{x}}$, where $i = 1, \dots, m$, m is the number of measurements and $j = 1, \dots, n$, n is the number of states to simplify the notations.

Algorithm 6.2

For the model (6.20), the following recursions are used and initialized with $\hat{x}_{1|0}$ and $P_{1|0}$:

1. Measurement update.

$$\hat{x}_{k|k} = \hat{x}_{k|k-1} + K_k \epsilon_k \quad (6.23)$$

$$\begin{aligned} P_{k|k} &= P_{k|k-1} \\ &\quad - P_{k|k-1} (h'_x(\hat{x}_{k|k-1}))^T S_k^{-1} h'_x(\hat{x}_{k|k-1}) P_{k|k-1} \end{aligned} \quad (6.24)$$

2. Time update.

$$\hat{x}_{k+1|k} = f(\hat{x}_{k|k}) \quad (6.25)$$

$$P_{k+1|k} = f'_x(\hat{x}_{k|k}) P_{k|k} (f'_x(\hat{x}_{k|k}))^T + Q_k \quad (6.26)$$

Where the innovation is defined as

$$\epsilon_k = y_k - h(\hat{x}_{k|k-1}) \quad (6.27)$$

for the innovation covariance is given by

$$S_k = h'_x(\hat{x}_{k|k-1}) P_{k|k-1} (h'_x(\hat{x}_{k|k-1}))^T + R_k \quad (6.28)$$

and Kalman gain is defined as

$$K_k = P_{k|k-1} (h'_x(\hat{x}_{k|k-1}))^T S_k^{-1} \quad (6.29)$$

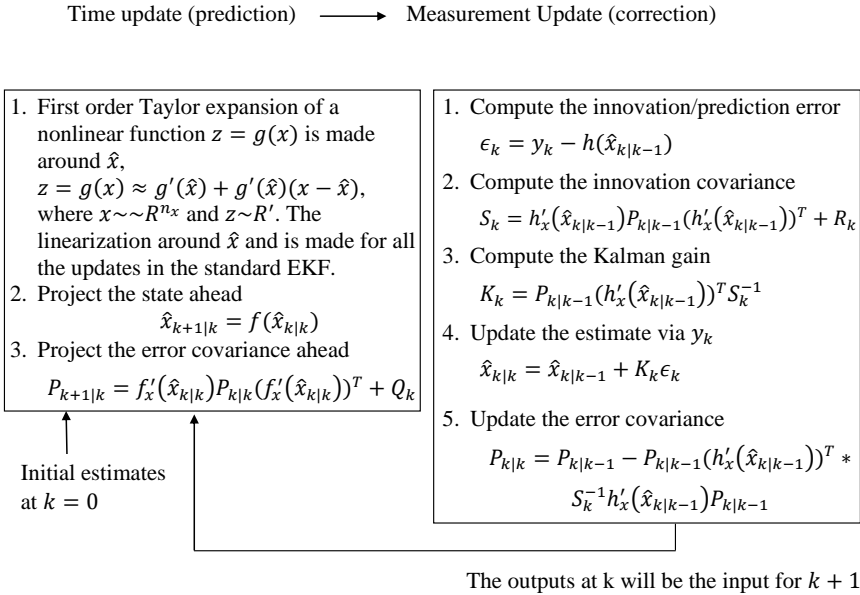


Figure 6.2. Extended Kalman filter: Overview of the calculation.

6.5 Overview of the Calculations in the EKF

An overview of the calculation in the EKF can be seen in figure 6.2. In step 1 in the time update first order Taylor expansion of a nonlinear function $z=g(x)$ is made around the current estimate state \hat{x} ,

$$z = g(x) \approx g(\hat{x}) + g'(\hat{x})(x - \hat{x}), \quad (6.30)$$

where $x \sim \mathcal{R}^{n_x}$ and (initially for notational convenience) $z \sim \mathcal{R}^1$. $g'(\hat{x})$ denotes the Jacobian evaluated at \hat{x} and this can be related to a linear state space model by the Kalman filter. The linearization around the current estimate state \hat{x} is made for all the updates in the standard EKF. After the linearization the states are estimated in the EKF in a similar way as the KF, compare figure 6.2 and figure 6.1.

6.6 Alternative Filters

The reason why an EKF is selected is to provide a simple way of weighting together different measurement signals. Another reason is that the equations of the model in chapter 8 do not contain as many nonlinearities and therefore a more advanced filter such as particle filter (PF) will not be needed. The purpose of this section is

that it will give a brief introduction to alternative filters that can be used instead of the EKF. This section is based on information from [31] and [29].

The goal with unscented Kalman filter (UKF) [32], [33] is to fit a Gaussian distribution at each time step. This is done by propagating a number of points in the state space. UKF is often more accurate than EKF. This is mainly because the quadratic term is accommodated in nonlinear models. Two other variants of this principle are the divided difference filter (DDF) [34] and the quadrature Kalman filter (QKF). Once again, these filters are bounded to be applied to posterior distributions that are unimodal.

Gaussian sum Kalman filters (GS-KF) presented in [35] can handle multimodal posteriors. The filters include a Gaussian mixture distribution and the posterior. An extension of this idea is the Kalman filter approximations such as the Gaussian sum quadrature Kalman filter (GS-QKF) in [36].

In [35], [37] the point mass filter (PMF) is described. The filter estimates the state recursively by gridding the state space and computing the posterior. PMF is able to represent any posterior distribution. The filter also applies to any nonlinear and non-Gaussian model. The algorithm is of quadratic complexity in the grid size.

Notice that the model is an approximation using Gaussian distributions as the posterior and this is both propagated by EKF and UKF. The PMF, on the other hand, approximates the posterior over a grid and uses the original model. Similar to the PMF, a numerical approximation to the nonlinear filtering problem is also outputted by the PF. The PF uses a stochastic grid that is adaptive. In the state space relevant grid points from the adaptive stochastic grid are automatically selected. It should also be mentioned that the standard PF has linear complexity in the number of grid points compared to the PMF.

Chapter 7

Model

The system model, see figure 1.1 is a modified and extended version of a model called Single Track Model with Road Interaction (STMRI). The STMRI is normally used for autonomous driving and lane keeping and is described by [38]. A deeper description and more information about STMRI and its equations can be found in [39] and [40]. The equations for the lane positioning state space model are in discrete state space form. To go from continuous form to discrete form Euler's method has been used. Euler's method is described in e.g. [41]. The state space vector for the system, see figure 1.1, is estimated by a KF with the measurement signals from the vehicle sensors (yaw rate, velocity, steering wheel angle), LPS system (camera), map data and GPS. The KF can be implemented in Matlab.

7.1 Single Track Model with Road Interaction

The vehicle motion is described with respect to a road fixed coordinate frame. The relative angle between vehicle and road is ψ_{RE} and is according to Ackermann's steering geometry described by

$$\dot{\psi}_{RE} = v_x c_0 + \dot{\psi}_E,$$

where the inverse of the road's radius gives the current curvature of the road, $c_0 = 1/R$. The yaw rate $\dot{\psi}_E$ is computed as

$$\dot{\psi}_E = \frac{v_x}{l_b} \delta_f,$$

where l_b is the wheel base of the vehicle and v_x is the ego vehicle's longitudinal velocity. To get the relative angle between vehicle and road ψ_{RE} the LPS system in the vehicle measures heading angle right χ_R and the heading angle left χ_L . The mean value between χ_R and χ_L is equal to ψ_{RE} , see figure 7.1.

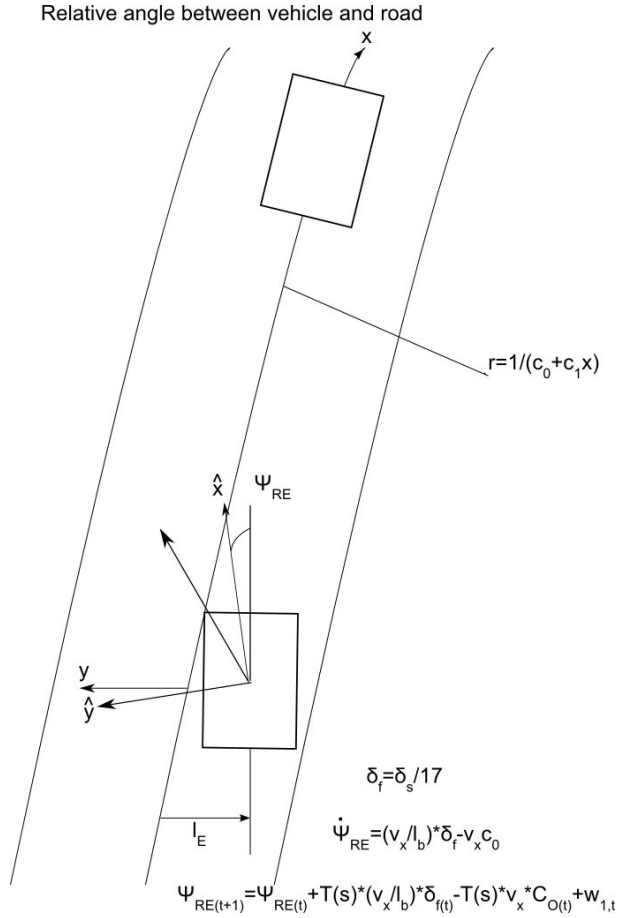


Figure 7.1. The relative angle between vehicle and road is ψ_{RE} . In the body coordinate system, (\hat{x}, \hat{y}) is the position of the moving vehicle. The position (x, y) in the curved coordinate system follows and is attached to the road. The lateral displacement of the vehicle in lane is l_E . The radius of the road is R and the current curvature of the road is c_0 . The derivative of the current curvature of the road is c_1 .

The lateral displacement of the vehicle in lane l_E has the following relation

$$\dot{l}_E = v_x \sin(\psi_{RE}) \approx v_x \psi_{RE}$$

for small angles of ψ_{RE} .

The front wheel angle δ_f and the steering wheel angle δ_s has the following relation

$$\delta_f = \frac{\delta_s}{\delta_k},$$

where δ_k is a constant, which depends on the referred vehicle. This constant δ_k is equal to 17 for the test vehicle mentioned in chapter 5.1.

A transition curve, whose curvature c changes linearly with its curve length x_c is described as a clothoid and gives the relation

$$c(x_c) = c_0 + c_1 x_c.$$

Suppose $x_c = 0$ at the position of the ego vehicle, in other words x_c is fixed to the ego vehicle. c_0 and c_1 will be time varying state variables when driving along the road and passing through different road segments. A curvature change in the transition curve at the position of the vehicle gives the relation

$$\frac{dc(x_c)}{dt} = \dot{c}_0 = \frac{dc_0}{dx_c} \frac{dx_c}{dt} = c_1 v_x,$$

where v_x is the ego vehicle's longitudinal velocity. To get the curvature at the ego vehicle c_0 , the LPS system in the vehicle measure the curvature right c_{0R} and the curvature left c_{0L} and the mean value between c_{0R} and c_{0L} is equal to c_0 . See figure 7.1.

7.2 State Space Model for the complete Lane Positioning System

The following dynamic discrete time state space equations describes the position of the vehicle in the lane:

$$\psi_{RE(t+1)} = \psi_{RE(t)} + T * v_x * c_{0(t)} + T * \dot{\psi}_E + w_{1,t} \tag{7.1}$$

$$l_{E(t+1)} = l_{E(t)} + T * v_x * \psi_{RE(t)} + w_{2,t} \tag{7.2}$$

$$\delta_{s(t+1)} = \delta_{s(t)} + w_{3,t} \tag{7.3}$$

$$\delta_{s(t+1)}^{offs} = \delta_{s(t)}^{offs} + w_{4,t} \tag{7.4}$$

$$c_{0(t+1)} = c_{0(t)} + T * v_x * c_{1(t)} + w_{5,t} \tag{7.5}$$

$$c_{1(t+1)} = c_{1(t)} + w_{6,t} \tag{7.6}$$

The definitions of ψ_{RE} , l_E , δ_s , c_0 , c_1 , v_x and $\dot{\psi}_E$ are described in section 7.1 and δ_s^{offs} in section 7.2.1. The KF in the lane position system, see figure 1.1 is based on the lane positioning system state space model described in this section, which gives the following state space vector

$$[\psi_{RE}, l_E, \delta_s, \delta_s^{offs}, c_0, c_1].$$

All the states in the state space vector are initialised with their first measurement signal except the curvature and its derivate, that are initialised to zero. This model of the position of the vehicle in the lane is linear and can be estimated by a KF. Chapter 8 describes an extended version of this lane positioning system state space model. The extended lane positioning system state space model has nonlinear state equations and therefore an EKF has been chosen.

7.2.1 Complete Measurement Equations

The steering wheel angle measurement has an offset and is a state variable in the model. The steering wheel angle offset δ_s^{offs} has the following relation

$$\delta_s^m = \delta_s + \delta_s^{offs}$$

where the measured steering wheel angle is δ_s^m . Position and time from GPS have been loaded into Volvo's map data program, which gives curvature and time in order to match map data with the other signals in the lane positioning system state space model. The GPS position is in WGS 84 coordinates, which is described in section 3.3. The measurements used in the KF are relative angle between vehicle and road, lateral displacement of vehicle in lane, steering wheel angle, curvature from LPS system, curvature from map data and GPS position in order to match it with correct curvature and have the following linear measurement equations

$$\psi_{RE_{measured,(t+1)}} = \psi_{RE_{(t+1)}} + v_{1,(t+1)} \quad (7.7)$$

$$l_{E_{measured,(t+1)}} = l_{E_{(t+1)}} + v_{2,(t+1)} \quad (7.8)$$

$$\delta_{s_{measured,(t+1)}} = \delta_{s_{(t+1)}} + \delta_{s_{(t+1)}}^{offs} + v_{3,(t+1)} \quad (7.9)$$

$$c_{0_{measured,(t+1)}} = c_{0_{(t+1)}} + v_{4,(t+1)} \quad (7.10)$$

$$c_{0_{mapdata_{measured,(t+1)}}} = c_{0_{mapdata_{(t+1)}}} + v_{5,(t+1)} \quad (7.11)$$

$$x_{measured,(t+1)} = x_{(t+1)} + v_{6,(t+1)} \quad (7.12)$$

$$y_{measured,(t+1)} = y_{(t+1)} + v_{7,t+1} \quad (7.13)$$

, where v_k , for $k = 1, 2 \dots 7$, is measurement noise.

Chapter 8

Extended Model

The model from chapter 7 can be extended. More reliable measurement signals from additional sensor sources give a more accurate position of the vehicle in the lane. The extended model and its equations and signals will be described in this chapter.

8.1 GPS and DR Model

The absolute position from the GPS is important to know in order to match the position with the road attributes from map data. In order to get a more accurate absolute position and avoid certain drawbacks with GPS, discussed in chapter 4.3, a DR model will be used together with the GPS. These complementary characteristics indicate that integration of a DR system and GPS can be advantageous. This integration will be done using an EKF.

The DR model is a dynamic model with constant speed and the following state space vector $x(t)$

$$x(t) = \begin{bmatrix} X(t) \\ Y(t) \\ \psi_E \end{bmatrix}$$

with it's derivative

$$\dot{x}(t) = \begin{bmatrix} v_x \cos \psi_E \\ v_x \sin \psi_E \\ \dot{\psi}_E \end{bmatrix}$$

Assuming constant velocity and yaw rate, the discrete time formulas are

$$X_{(t+1)} = X_{(t)} + T v_x \cos \psi_{E(t)} \quad (8.1)$$

$$Y_{(t+1)} = Y_{(t)} + T v_x \sin \psi_{E(t)} \quad (8.2)$$

$$\psi_{E(t+1)} = \psi_{E(t)} + T \dot{\psi}_{E(t)} \quad (8.3)$$

that in a NEZ frame, see chapter 3.4, have the following expressions

$$N_{(t+1)} = N_{(t)} + Tv_{(x)}\cos\psi_{E_{(t)}} \quad (8.4)$$

$$E_{(t+1)} = E_{(t)} + Tv_{(x)}\sin\psi_{E_{(t)}} \quad (8.5)$$

$$\psi_{E_{(t+1)}} = \psi_{E_{(t)}} + T\dot{\psi}_{E_{(t)}} \quad (8.6)$$

The expressions are based on small changes in yaw during one sample interval. Note the assumption that there are no lateral velocity in the DR model. There are different approaches of calculating a vehicle's absolute position. Since the GPS has slow sample frequency, the approach here, is that the DR measurements are estimated by the EKF, every time the EKF does not have GPS measurements. In this thesis a DR system and a GPS receiver will be integrated with an EKF. To compare the absolute position from the GPS with the calculated position from the DR, the GPS position can be transformed from WGS 84 to UTM coordinates or RT90. Transformation to RT90 coordinates has been chosen to be able to compare data with SNRA data.

8.2 Constant Velocity Model

This model is called constant velocity model and has the following equations in continuous time.

The state space vector

$$x(t) = \begin{bmatrix} p(t) \\ v(t) \end{bmatrix}$$

where $p(t)$ denotes the position in 2D (N, E).

By definition the position's derivative is equal to the longitudinal velocity

$$\dot{p}_x = v_x$$

where the longitudinal velocity's derivative \dot{v}_x is modeled by the following relation

$$\dot{v}_x = w.$$

The next state of velocity's derivative is unknown and to cover the errors in the model, the next state of velocity's derivative has been set to gaussian white noise w with mean value equal to zero.

8.3 Coordinated Turn Model

This model is called coordinated turn model and is based on the same principles as the constant acceleration model, described in [29]. The state space vector is

$$x(t) = \begin{bmatrix} \psi_E \\ \dot{\psi}_E \\ \ddot{\psi}_E \end{bmatrix}.$$

If $p(t)$ is given by yaw angle ψ_E . The following relation will hold

$$p(t) = \psi_E$$

The yaw angle's derivative is defined by following relation

$$\dot{\psi}_E = W$$

where W is the angular velocity.

The angular velocity is defined by the following relation

$$\dot{W} = \alpha$$

where α is the angular acceleration. The angular acceleration has the following relation

$$\dot{\alpha} = w$$

In a comparison between the constant acceleration model and the coordinated turn model it is seen that they are based on the same principles, the only difference here in the coordinated turn model is that this model has an angular velocity and angular acceleration instead of a velocity and an acceleration as in the constant acceleration model, which explains the following two states.

The yaw rate $\dot{\psi}_E$ has the following trivial relation

$$\dot{\dot{\psi}}_E = \dot{\psi}_E.$$

$\dot{\dot{\psi}}_E$ is the next state of yaw rate $\dot{\psi}_E$ and defined as

$$\dot{\dot{\psi}}_E = w.$$

The next state of yaw rate's derivative is unknown and to cover the errors in the model, the next state of yaw rate's derivative has been set to white noise with expected value w .

8.4 State Space Model for the complete Extended Lane Positioning System

The equations describing the extended model give the following dynamic time discrete equations

$$\psi_{RE(t+1)} = \psi_{RE(t)} + Tv_{x(t)}c_{0(t)} - T\dot{\psi}_{E(t)} + w_{1,t} \tag{8.7}$$

$$l_{E(t+1)} = l_{E(t)} + Tv_{x(t)}\psi_{RE(t)} + w_{2,t} \tag{8.8}$$

$$c_{0(t+1)} = c_{0(t)} + Tv_{x(t)}c_{1(t)} + w_{3,t} \tag{8.9}$$

$$c_{1(t+1)} = c_{1(t)} + w_{4,t} \tag{8.10}$$

$$N_{(t+1)} = N_{(t)} + Tv_{(x)}\cos\psi_{E(t)} + w_{5,t} \tag{8.11}$$

$$E_{(t+1)} = E_{(t)} + Tv_{(x)}\sin\psi_{E(t)} + w_{6,t} \tag{8.12}$$

$$v_{x(t+1)} = v_{x(t)} + w_{7,t} \tag{8.13}$$

$$\psi_{E(t+1)} = \psi_{E(t)} + T\dot{\psi}_{E(t)} + w_{8,t} \tag{8.14}$$

$$\dot{\psi}_{E(t+1)} = \dot{\psi}_{E(t)} + w_{9,t} \tag{8.15}$$

The definitions of ψ_{RE} , l_E , c_0 , c_1 , v_x and $\dot{\psi}_E$ are described in section 7.1 and the definitions of N , E , v_x , ψ_E , $\dot{\psi}_E$ are described in section 8.2, 8.3 and 8.4. An extended and modified version of the model, described in section 7, has been implemented in Matlab. The EKF in the extended model is based on the signal model described in the previous section, which gives the following state space vector

$$[\psi_{RE}, l_E, c_0, c_1, N, E, v_x, \psi_E, \dot{\psi}_E].$$

All states in the state space vector are initialised with their first measurement signal except curvature and its derivate, that are initialised to zero. The extended model has nonlinear state equations and therefore an EKF has been chosen.

8.4.1 Complete Extended Measurement Equations

To compare the absolute position from the GPS with the calculated position from the DR, the GPS position can be transformed from WGS 84 to UTM or RT90 coordinates. Transformation to RT90 coordinates has been chosen to be able to compare data with SNRA data. Position and time have been loaded into Volvo's map data program, which gives curvature and time in order to match map data with the other signals in the extended lane positioning system state space model. The measurements in the EKF are relative angle between vehicle and road, lateral displacement of the vehicle in the lane, steering wheel angle, curvature from LPS system, curvature from map data and GPS position in order to match it with correct curvature from map data and have the following linear measurements equations

$$\psi_{RE_{measured,(t+1)}} = \psi_{RE_{(t+1)}} + v_{1,(t+1)} \quad (8.16)$$

$$l_{E_{measured,(t+1)}} = l_{E_{(t+1)}} + v_{2,(t+1)} \quad (8.17)$$

$$c_{0_{measured,(t+1)}} = c_{0_{(t+1)}} + v_{3,(t+1)} \quad (8.18)$$

$$c_{0_{mapdata_{measured,(t+1)}}} = c_{0_{mapdata_{(t+1)}}} + v_{4,(t+1)} \quad (8.19)$$

$$N_{measured,(t+1)} = x_{(t+1)} + v_{5,(t+1)} \quad (8.20)$$

$$E_{measured,(t+1)} = y_{(t+1)} + v_{6,t+1} \quad (8.21)$$

$$v_{x_{measured,(t+1)}} = v_{x_{(t+1)}} + v_{7,t+1} \quad (8.22)$$

$$\dot{\psi}_{E_{measured,(t+1)}} = \dot{\psi}_{E_{(t+1)}} + v_{8,t+1} \quad (8.23)$$

$$GPS_{heading_{measured,(t+1)}} = \psi_{E_{(t+1)}} + v_{9,t+1} \quad (8.24)$$

$$\frac{v_{x_{measured,(t+1)}} * \delta_{s_{measured,(t+1)}}}{l_b} = \dot{\psi}_{E_{(t+1)}} + v_{10,t+1} \quad (8.25)$$

, where v_k , for $k = 1, 2 \dots 10$, is measurement noise.

Chapter 9

Results

The aim of this thesis was to investigate the performance of a lane position monitoring system (described in chapter 1.3) and investigate enhancement techniques for increasing the robustness and availability of such a system by using additional sensor sources like map data and GPS. This chapter presents the results of the investigation and Root Mean Square (RMS) values, described in chapter 9.5 is used to evaluate the performance of the lane position monitoring system. In order to investigate whether the robustness and availability of such a system, using additional sensor sources like map data, increase, four techniques described in chapter 9.1, 9.2, 9.3 and 9.4 are introduced. Two data sequences, Data sequence 1 and Data sequence 2, described in chapter 5.1.1 and chapter 5.1.2, and three cases, Case A, B and C are also used. The EKF is described in chapter 6. Case A is when the curvature without map data is estimated by the EKF. Case B is when the curvature with map data is estimated by the EKF and Case C is when the curvature both with map data and with reliable camera data is estimated by the EKF. The author evaluated the solution offline using simulations and a signal that indicates if the LPS system has reliable camera data over a large sequence has been manually added to the system estimated by the EKF in the measurement update. There is a signal from the lane positioning sensor (LPS) system that indicates if the camera data is reliable and could be used for an online solution.

9.1 Technique 1: Curvature and Position Compared with Data from the Swedish National Road Administration

To be able to compare the estimated curvature from the EKF with data from Vägverket (Swedish National Road Administration, SNRA), the distance between one GPS position as estimated by the EKF and the GPS positions from SNRA are calculated. The GPS positions estimated by the EKF are referred to as *GPSF*, with coordinates \hat{x}_{GPS} and \hat{y}_{GPS} , and the GPS positions from SNRA, referred to as *GPSV*, with coordinates x_{GPSV} and y_{GPSV} . One data point from the EKF

is said to "match" one of the data points from SNRA, if the distance between the two positions is less than a constant C , i.e.

$$\|GPSV - GPSF\| = \sqrt{(x_{GPSV} - \hat{x}_{GPS})^2 + (y_{GPSV} - \hat{y}_{GPS})^2} < C. \quad (9.1)$$

Every time a match between the positions has been found the estimated curvature by the EKF and SNRA are saved and compared. Initially, the EKF estimated the curvature without map data for Data sequence 1, as seen in figure 9.1 and subsequently the EKF estimated the curvature with map data for Data sequence 1, as shown in figure 9.2. A similiar comparison has been made for Data sequence 2, where the EKF estimated the curvature without map data, figure 9.3 and additionally with map data, figure 9.4 and finally with map data and reliable camera data, figure 9.5.

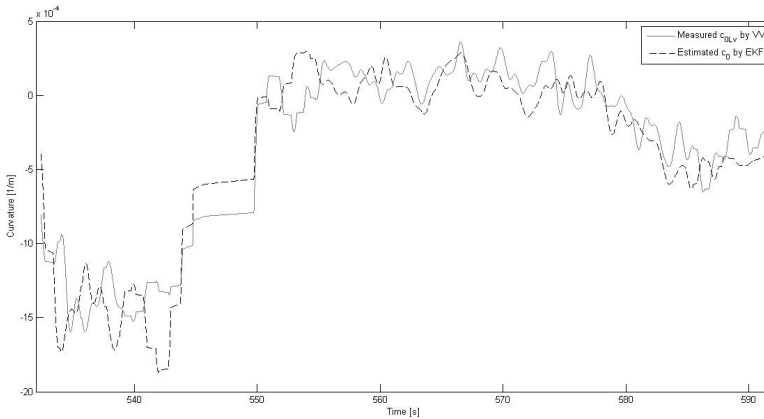


Figure 9.1. Comparison between the measured curvature from SNRA c_{0LV} (gray) and the estimated curvature without map data from the EKF c_0 (black dashed) for Data sequence 1, as described in chapter 5.1.1 and according to technique 1. Note that the scale is very small ($1 * 10^{-4}$), resulting in small changes in time have a large effect in the curvature.

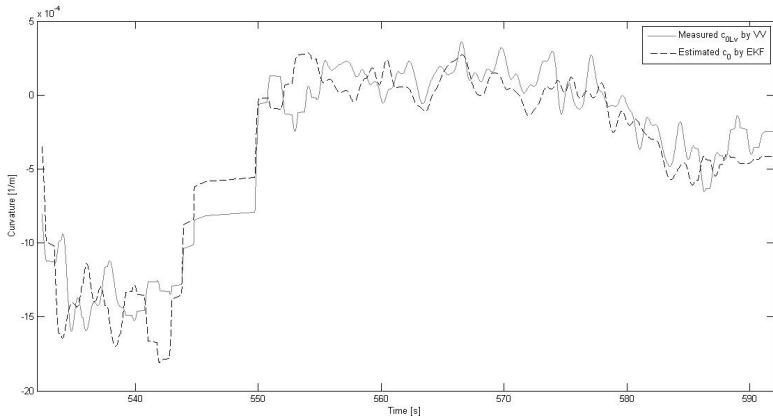


Figure 9.2. Comparison between the measured curvature from SNRA c_{0LV} (gray) and the estimated curvature with map data from the EKF c_0 (black dashed) for Data sequence 1, as described in chapter 5.1.1 and according to technique 1. Note that the scale is very small (1×10^{-4}), resulting in small changes in time have a large effect in the curvature.

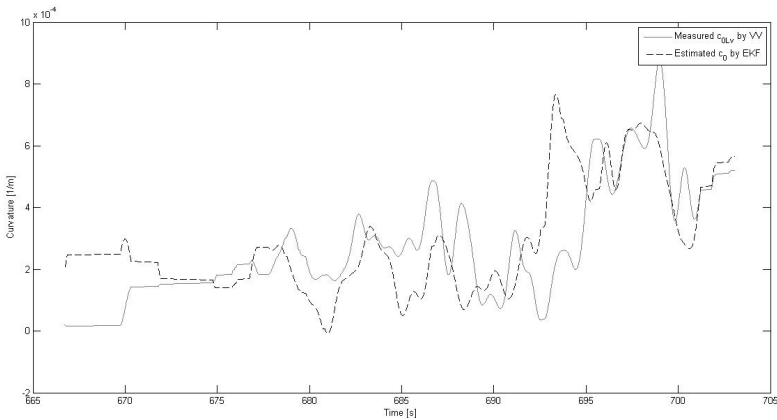


Figure 9.3. Comparison between the measured curvature from SNRA c_{0LV} (gray) and the estimated curvature without map data from the EKF c_0 (black dashed) for Data sequence 2, as described in chapter 5.1.2 and according to technique 1. Note that the scale is very small (1×10^{-4}), resulting in small changes in time have a large effect in the curvature.

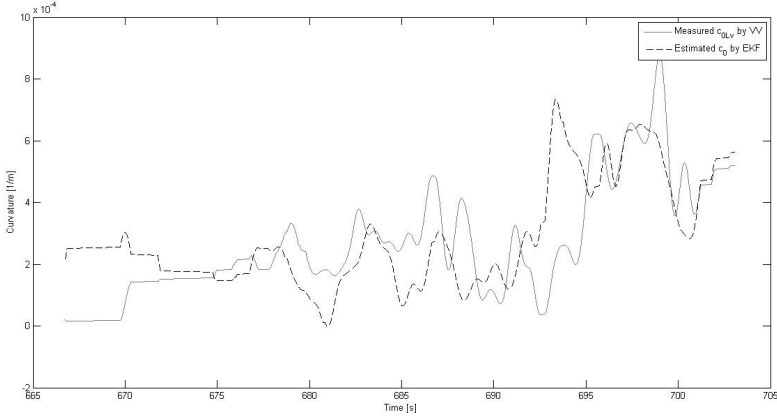


Figure 9.4. Comparison between the measured curvature from SNRA c_{0LV} (gray) and the estimated curvature with map data from the EKF c_0 (black dashed) for Data sequence 2, as described in chapter 5.1.2 and according to technique 1. Note that the scale is very small ($1 * 10^{-4}$), resulting in small changes in time have a large effect in the curvature.

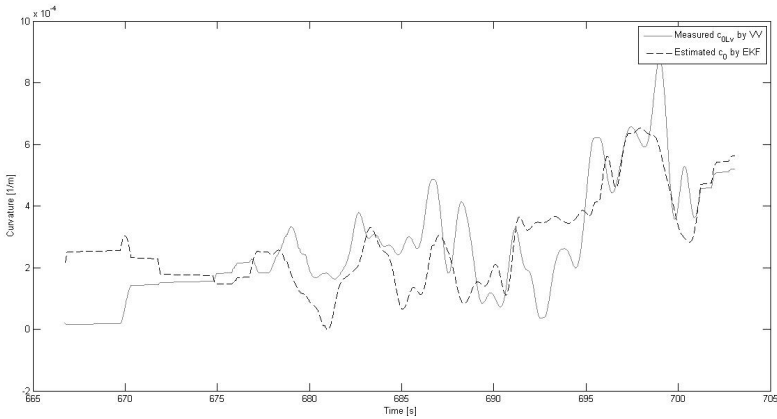


Figure 9.5. Comparison between the measured curvature from SNRA c_{0LV} (gray) and the estimated curvature with map data and reliable camera data from the EKF c_0 (black dashed) for Data sequence 2, as described in chapter 5.1.2 and according to technique 1. Note that the scale is very small ($1 * 10^{-4}$), resulting in small changes in time have a large effect in the curvature.

9.2 Technique 2: Curvature and Distance Compared with Data from the Swedish National Road Administration

The curvature of one data point of the EKF is compared to that of a matching data point from SNRA, as described by equation 9.1. The estimated distance, s , measured in metres, from the EKF in chapter 6 is calculated for Data sequence 1 and 2 in chapter 5.1.1 and 5.1.2. According to

$$s_i = \sum_{j=1}^{i+1} v_{xj} * \Delta t, \tag{9.2}$$

where s_i is the distance between data point i and $i + 1$, the longitudinal velocity v_{xj} is estimated from the EKF and the time Δt is the EKF simulation time step, here equal to 0.01 s.

The estimated distance s and the distance from SNRA, defined as s_v , are linearly interpolated, giving the matching estimated curvature c_0 from the EKF and the curvature c_{0Lv} from SNRA. Initially, the EKF estimated the curvature without map data for Data sequence 1, as seen in figure 9.6, and for Data sequence 2 in figure 9.8. Furthermore the EKF estimated the curvature with map data, as shown in figure 9.7 for Data sequence 1 and in figure 9.9 for Data sequence 2. Finally the EKF estimated the curvature with map data and reliable camera data, see figure 9.10 for Data sequence 2.

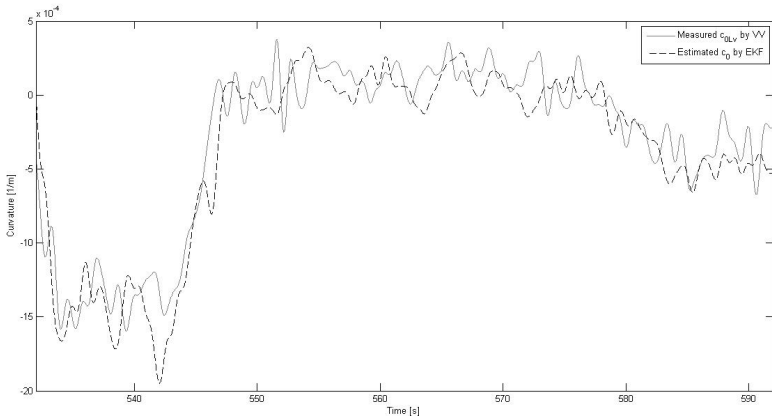


Figure 9.6. Comparison between the measured curvature from SNRA c_{0Lv} (gray) and the estimated curvature without map data from the EKF c_0 (black dashed) for Data sequence 1, as described in chapter 5.1.1 and according to technique 2. Note that the scale is very small ($1 * 10^{-4}$), resulting in small changes in time have a large effect in the curvature.

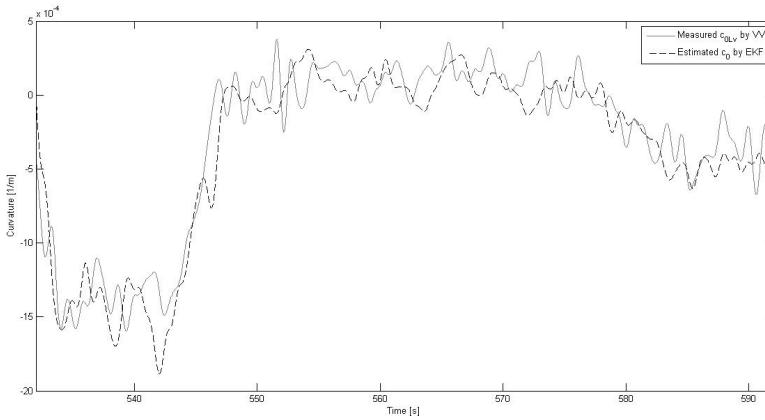


Figure 9.7. Comparison between the measured curvature from SNRA c_{0LV} (gray) and the estimated curvature with map data from the EKF c_0 (black dashed) for Data sequence 1, as described in chapter 5.1.1 and according to technique 2. Note that the scale is very small ($1 * 10^{-4}$), resulting in small changes in time have a large effect in the curvature.

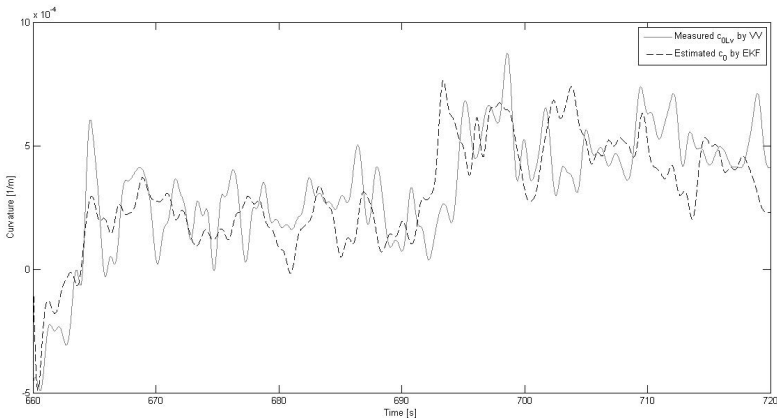


Figure 9.8. Comparison between the measured curvature from SNRA c_{0LV} (gray) and the estimated curvature without map data from the EKF c_0 (black dashed) for Data sequence 2, as described in chapter 5.1.2 and according to technique 2. Note that the scale is very small ($1 * 10^{-4}$), resulting in small changes in time have a large effect in the curvature.

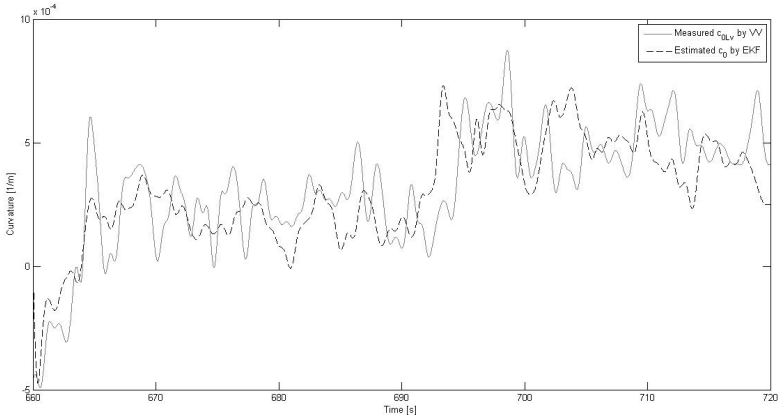


Figure 9.9. Comparison between the measured curvature from SNRA c_{0LV} (gray) and the estimated curvature with map data from the EKF c_0 (black dashed) for Data sequence 2, as described in chapter 5.1.2 and according to technique 2. Note that the scale is very small ($1 * 10^{-4}$), resulting in small changes in time have a large effect in the curvature.

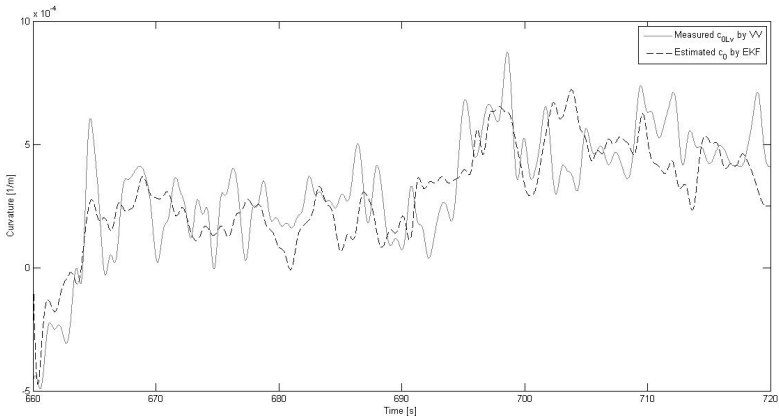


Figure 9.10. Comparison between the measured curvature from SNRA c_{0LV} (gray) and the estimated curvature with map data and reliable camera data from the EKF c_0 (black dashed) for Data sequence 2, as described in chapter 5.1.2 and according to technique 2. Note that the scale is very small ($1 * 10^{-4}$), resulting in small changes in time have a large effect in the curvature.

9.3 Technique 3: Curvature and Time Compared with the Data from the Swedish National Road Administration

The data from the SNRA in chapter 5.1.6 is sampled per metre. A match for the norm between the first GPS position, $GPSF$, is estimated from the EKF, and the GPS position from the SNRA, $GPSV$, are found according to equation 9.1. The distance between two of SNRA's data points is one metre. Thus the average velocity between two data points can be calculated. Then the time t_v is calculated according to

$$t_{vi} = \sum_{j=0}^i \left(\frac{1}{\frac{v_{x_i} + v_{x_{i-1}}}{2}} \right), \quad (9.3)$$

where t_i is the time between data points $i - 1$ and i , the longitudinal velocity v_{x_i} is estimated from the EKF in chapter 6. The time t_v from the SNRA and the time t from the EKF are linearly interpolated, resulting in the matching estimated curvature c_0 from the EKF and the curvature c_{0LV} from SNRA. Initially, the EKF estimated the curvature without map data for Data sequence 1, as seen in figure 9.11, and for Data sequence 2, figure 9.13. Subsequently the EKF estimated the curvature with map data, figure 9.12 for Data sequence 1 and figure 9.14 for Data sequence 2. Finally the EKF estimated the curvature with map data and reliable camera data, as shown in figure 9.15 for Data sequence 2.

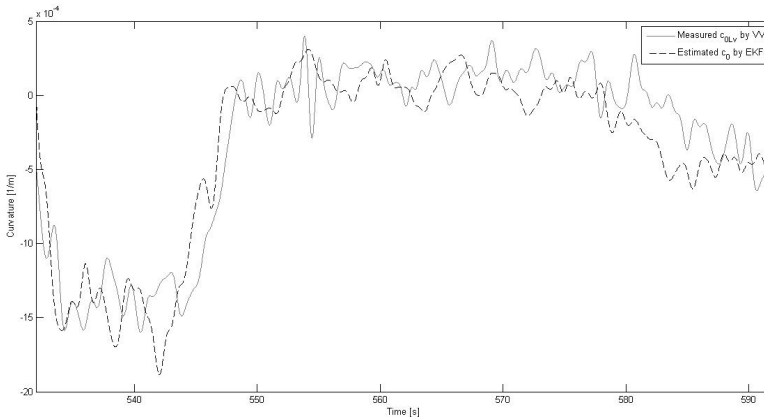


Figure 9.12. Comparison between the measured curvature from SNRA c_{0LV} (gray) and the estimated curvature with map data from the EKF c_0 (black dashed) for Data sequence 1, as described in chapter 5.1.1 and according to technique 3. Note that the scale is very small ($1 * 10^{-4}$), resulting in small changes in time have a large effect in the curvature.

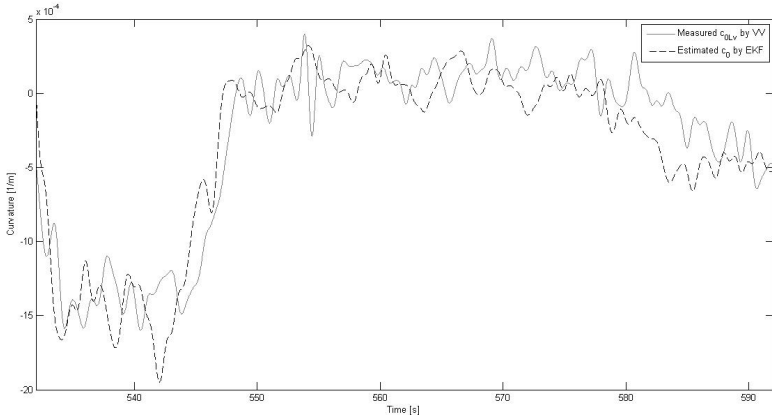


Figure 9.11. Comparison between the measured curvature from SNRA c_{0LV} (gray) and the estimated curvature without map data from the EKF c_0 (black dashed) for Data sequence 1, as described in chapter 5.1.1 and according to technique 3. Note that the scale is very small ($1 * 10^{-4}$), resulting in small changes in time have a large effect in the curvature.

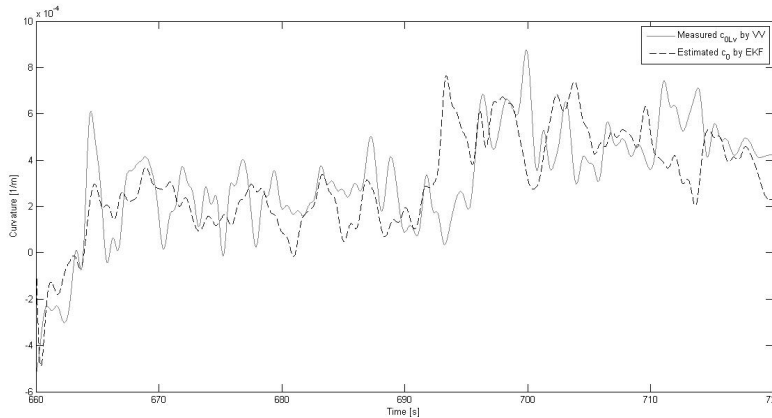


Figure 9.13. Comparison between the measured curvature from SNRA c_{0LV} (gray) and the estimated curvature without map data from the EKF c_0 (black dashed) for Data sequence 2, as described in chapter 5.1.2 and according to technique 3. Note that the scale is very small ($1 * 10^{-4}$), resulting in small changes in time have a large effect in the curvature.

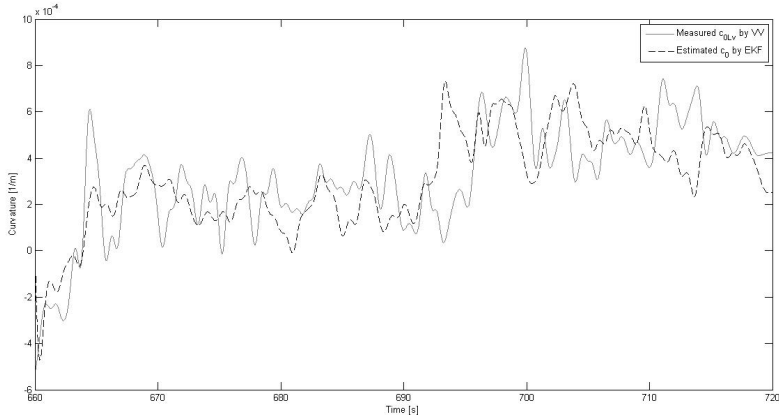


Figure 9.14. Comparison between the measured curvature from SNRA c_{0LV} (gray) and the estimated curvature without map data from the EKF c_0 (black dashed) for Data sequence 2, as described in chapter 5.1.2 and according to technique 3. Note that the scale is very small ($1 * 10^{-4}$), resulting in small changes in time have a large effect in the curvature.

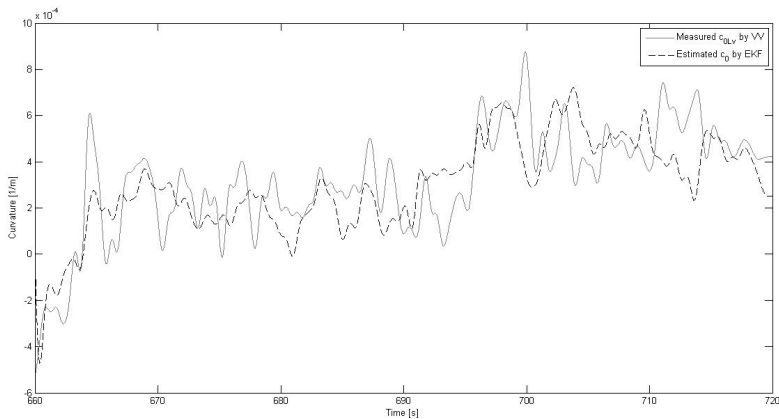


Figure 9.15. Comparison between the measured curvature from SNRA c_{0LV} (gray) and the estimated curvature with map data and reliable camera data from the EKF c_0 (black dashed) for Data sequence 2, as described in chapter 5.1.2 and according to technique 3. Note that the scale is very small ($1 * 10^{-4}$), resulting in small changes in time have a large effect in the curvature.

9.4 Technique 4: Curvature and Position Compared with Data from the Swedish National Road Administration

Technique 4 will be divided into three subtechniques. Initially, the GPS positions from the EKF and the GPS positions from SNRA are compared. Every time the nearest match between the positions from the EKF and SNRA has been found the corresponding estimated curvature by the EKF and SNRA are saved and compared. 31269 matching GPS points have been found between the GPS positions from the EKF and the GPS positions from SNRA. This subtechnique will be referred to as T4GPS. After the best norm has been chosen as the starting point in the same way as in T4GPS, distance and time are calculated in the same way as in section 9.2 and 9.3. The estimated curvature by the EKF and SNRA are saved and compared as in section 9.2 and 9.3. These subtechniques will be referred to as T4Distance and T4Time. In figures B.1, B.6, B.11, the EKF estimated the curvature without map data for Data sequence 1 can be seen and the corresponding data for Data sequence 2 can be seen in figures B.3, B.8, B.13. Subsequently the EKF estimated the curvature with map data, figures B.2, B.7, B.12 for Data sequence 1 and figures B.4, B.9, B.14 for Data sequence 2. Finally the EKF estimated the curvature with map data and reliable camera data, as shown in figures B.5, B.10, B.15 for Data sequence 2.

9.5 Root Mean Square

RMS is used to investigate whether the availability and robustness of the lane positioning monitoring system increase when curvature from map data is used. The RMS value of a set of values is the square root of the arithmetic mean of the squares of the original values.

In the case of a set of n values $c_{01}, c_{02}, \dots, c_{0n}$, the RMS value is given by

$$c_{0rms} = \sqrt{\frac{1}{n}(c_{01}^2 + c_{02}^2 + \dots + c_{0n}^2)}, \tag{9.4}$$

where in this case n is the size of the array for the estimated curvature from the EKF in chapter 6 and the curvature from SNRA (see chapter 5.1.6) for all techniques 1-3. Here c_0 is defined as the difference between the estimated curvature and the curvature from SNRA for all techniques 1-3.

9.6 Summarization of Results

Table 9.1 and 9.2 summarizes RMS values and data for all investigations for techniques 1-3 combined with Data sequences 1-2 and cases A, B, C. In the tables Table 9.1 and 9.2, the techniques 1-3 will be abbreviated T1-T3 and Data sequences 1-2 will be referred to as D1-D2. The last column in table 9.2 shows, in percent, the improvement RMS values for Case B and C compared to Case A.

Table 9.3 summarizes the RMS values and data for all investigations for technique 4 and its subtechniques T4GPS, T4Distance and T4Time in a similar way.

Table 9.1. RMS values and data for all investigations.

Investigation	Figure	Number of GPS points	Number of duplicates	Norm
T1-D1-Case A	-	815	2	0.5 m
T1-D1-Case B	-	815	2	0.5 m
T1-D2-Case A	-	7	0	0.5 m
T1-D2-Case B	-	7	0	0.5 m
T1-D1-Case A	-	3257	1263	1 m
T1-D1-Case B	-	3257	1263	1 m
T1-D2-Case A	-	516	113	1 m
T1-D2-Case B	-	516	113	1 m
T1-D1-Case A	9.1	13894	9539	2 m
T1-D1-Case B	9.2	13894	9539	2 m
T1-D2-Case A	9.3	6639	4183	2 m
T1-D2-Case B	9.4	6639	4183	2 m

Table 9.2. RMS values and data for all investigations.

Investigation	Norm	Figure	RMS	Percent
T1-D1-Case A	0.5 m	-	$1.9397 * 10^{-4} m^{-1}$	-
T1-D1-Case B	0.5 m	-	$1.9149 * 10^{-4} m^{-1}$	1.28
T1-D2-Case A	0.5 m	-	$1.0089 * 10^{-4} m^{-1}$	-
T1-D2-Case B	0.5 m	-	$1.0309 * 10^{-4} m^{-1}$	-2.18
T1-D2-Case C	0.5 m	-	$1.0309 * 10^{-4} m^{-1}$	-2.18
T2-D1-Case A	0.5 m	-	$2.2100 * 10^{-4} m^{-1}$	-
T2-D1-Case B	0.5 m	-	$2.1403 * 10^{-4} m^{-1}$	3.15
T2-D2-Case A	0.5 m	-	$1.8552 * 10^{-4} m^{-1}$	-
T2-D2-Case B	0.5 m	-	$1.8077 * 10^{-4} m^{-1}$	2.56
T2-D2-Case C	0.5 m	-	$1.6949 * 10^{-4} m^{-1}$	8.64
T3-D1-Case A	0.5 m	-	$2.8212 * 10^{-4} m^{-1}$	-
T3-D1-Case B	0.5 m	-	$2.7600 * 10^{-4} m^{-1}$	2.17
T3-D2-Case A	0.5 m	-	$1.9453 * 10^{-4} m^{-1}$	-
T3-D2-Case B	0.5 m	-	$1.8956 * 10^{-4} m^{-1}$	2.55
T3-D2-Case C	0.5 m	-	$1.7594 * 10^{-4} m^{-1}$	9.56
T1-D1-Case A	1 m	-	$2.0220 * 10^{-4} m^{-1}$	-
T1-D1-Case B	1 m	-	$1.9827 * 10^{-4} m^{-1}$	1.94
T1-D2-Case A	1 m	-	$1.3134 * 10^{-4} m^{-1}$	-
T1-D2-Case B	1 m	-	$1.2811 * 10^{-4} m^{-1}$	2.46
T1-D2-Case C	1 m	-	$1.2812 * 10^{-4} m^{-1}$	2.45
T2-D1-Case A	1 m	-	$2.1941 * 10^{-4} m^{-1}$	-
T2-D1-Case B	1 m	-	$2.1247 * 10^{-4} m^{-1}$	3.16
T2-D2-Case A	1 m	-	$1.8530 * 10^{-4} m^{-1}$	-
T2-D2-Case B	1 m	-	$1.8079 * 10^{-4} m^{-1}$	2.43
T2-D2-Case C	1 m	-	$1.6958 * 10^{-4} m^{-1}$	8.48
T3-D1-Case A	1 m	-	$2.8663 * 10^{-4} m^{-1}$	-
T3-D1-Case B	1 m	-	$2.8078 * 10^{-4} m^{-1}$	2.04
T3-D2-Case A	1 m	-	$1.9441 * 10^{-4} m^{-1}$	-
T3-D2-Case B	1 m	-	$1.8971 * 10^{-4} m^{-1}$	2.42
T3-D2-Case C	1 m	-	$1.7532 * 10^{-4} m^{-1}$	9.82
T1-D1-Case A	2 m	9.1	$2.2301 * 10^{-4} m^{-1}$	-
T1-D1-Case B	2 m	9.2	$2.1709 * 10^{-4} m^{-1}$	2.65
T1-D2-Case A	2 m	9.3	$2.0026 * 10^{-4} m^{-1}$	-
T1-D2-Case B	2 m	9.4	$1.9634 * 10^{-4} m^{-1}$	1.96
T1-D2-Case C	2 m	9.5	$1.6824 * 10^{-4} m^{-1}$	15.99
T2-D1-Case A	2 m	9.6	$2.1923 * 10^{-4} m^{-1}$	-
T2-D1-Case B	2 m	9.7	$2.1290 * 10^{-4} m^{-1}$	2.89
T2-D2-Case A	2 m	9.8	$1.8173 * 10^{-4} m^{-1}$	-
T2-D2-Case B	2 m	9.9	$1.7728 * 10^{-4} m^{-1}$	2.45
T2-D2-Case C	2 m	9.10	$1.6846 * 10^{-4} m^{-1}$	7.30
T3-D1-Case A	2 m	9.11	$2.6321 * 10^{-4} m^{-1}$	-
T3-D1-Case B	2 m	9.12	$2.5816 * 10^{-4} m^{-1}$	1.92
T3-D2-Case A	2 m	9.13	$1.9294 * 10^{-4} m^{-1}$	-
T3-D2-Case B	2 m	9.14	$1.8774 * 10^{-4} m^{-1}$	2.70
T3-D2-Case C	2 m	9.15	$1.7190 * 10^{-4} m^{-1}$	10.90

Table 9.3. RMS values and data for all investigations of technique 4.

Investigation	Figure	RMS	Percent
T4GPS-D1-Case A	B.1	$2.3147 * 10^{-4} m^{-1}$	-
T4GPS-D1-Case B	B.2	$2.2567 * 10^{-4} m^{-1}$	2.51
T4GPS-D2-Case A	B.3	$1.9474 * 10^{-4} m^{-1}$	-
T4GPS-D2-Case B	B.4	$1.9042 * 10^{-4} m^{-1}$	2.22
T4GPS-D2-Case C	B.5	$1.7802 * 10^{-4} m^{-1}$	8.59
T4Distance-D1-Case A	B.6	$2.1941 * 10^{-4} m^{-1}$	-
T4Distance-D1-Case B	B.7	$2.1247 * 10^{-4} m^{-1}$	3.16
T4Distance-D2-Case A	B.8	$1.8564 * 10^{-4} m^{-1}$	-
T4Distance-D2-Case B	B.9	$1.8089 * 10^{-4} m^{-1}$	2.56
T4Distance-D2-Case C	B.10	$1.6955 * 10^{-4} m^{-1}$	8.67
T4Time-D1-Case A	B.11	$2.7425 * 10^{-4} m^{-1}$	-
T4Time-D1-Case B	B.12	$2.6877 * 10^{-4} m^{-1}$	2.00
T4Time-D2-Case A	B.13	$1.9449 * 10^{-4} m^{-1}$	-
T4Time-D2-Case B	B.14	$1.8977 * 10^{-4} m^{-1}$	2.43
T4Time-D2-Case C	B.15	$1.7609 * 10^{-4} m^{-1}$	9.46

Chapter 10

Conclusions and Future Work

This chapter is a summarization of conclusions from the results and evaluation of the lane positioning monitoring system presented in chapter 9. Some ideas for future work are also discussed.

10.1 Summary of Conclusions

The aim of this thesis was to investigate the performance of a lane position monitoring system and investigate enhancement techniques for increasing the robustness and availability of such a system by using additional sensor sources like map data and GPS.

The evaluation of RMS values in Table 9.2 showed that Case C gives up to almost 16 percent improvement of RMS values and Case B more than 3 percent improvement of RMS values compared to Case A, depending on which norm that is used in equation 9.1. Case A is when the curvature without map data is estimated by the EKF and Case B is when the curvature with map data is estimated by the EKF. Finally, Case C is when the curvature with map data and reliable camera data is estimated by the EKF.

Another aspect of the evaluation of RMS values in Table 9.2, is that technique 1 is more accurate than technique 2 and 3, since the RMS values is smaller for technique 1. The figures in chapter 9.2 and chapter 9.3, the evaluation of RMS values in table 9.1 showed that technique 2 gives more accurate information for the lane position monitoring system than technique 3. It is harder to draw conclusions from the pictures in chapter 9.1 since it depending on how many matching GPS positions between the estimated GPS positions by the EKF and the measured GPS positions by SNRA.

Table 9.1 showed that technique 1, described in chapter 9.1, had problems finding matching GPS positions between the estimated GPS positions by EKF and the measured GPS positions from SNRA for Data sequence 2 compared to

Data sequence 1. This depends on that the data is including disturbance in Data sequence 2, see chapter 5.1.2, compared to Data sequence 1, described in chapter 5.1.1. This means that it is harder for the EKF to estimate the position of the vehicle under disturbance, but even in this case the RMS values in Table 9.2 showed that Case C gives up to almost 16 percent improvement of RMS values and Case B gives up to almost three percent improvement of RMS values compared to Case A.

The negative values of the technique 1 when the standard is less than 0.5 m may be because a GPS point on the connecting road in Data sequence 2. Since Case B and C are dependent on each other the error occurs in both cases, but since technique 2, technique 3 and technique 4 showed improvement for Case B and Case C in Data sequence 2, the error can be considered as negligible.

The evaluation of RMS values in Table 9.3 showed that Case C gives up to more than nine percent improvement of RMS values and Case B more than 3 percent improvement of RMS values compared to Case A. An aspect of the evaluation of RMS values in Table 9.3, is that technique 1 is more accurate than technique 4, since the RMS values is smaller for technique 1. Similarly, subtechnique T4Time is more accurate than T4Distance and T4GPS, since the RMS values is smaller for subtechnique T4GPS. The figures in chapter B.1.2 and chapter B.1.1, the evaluation of RMS values in table 9.3 showed that subtechnique T4Distance gives more accurate information for the lane position monitoring system than subtechnique T4GPS.

The data from the SNRA is not optimal since it needs to be preprocessed, see chapter 5.1.6, but it the best comparing data that was given to this thesis to evaluate the EKF. The SNRA data fullfills its purpose but in future work it can be an idea to consider which comparing data is used or collecting specific data to evaluate the EKF.

In the beginning of this thesis, the inputs and measurement signals from the vehicle sensors (yaw rate, velocity, steering wheel angle), LPS system (camera), map data and GPS, were sent to the developed sensor fusion model. The discrete part of the logged data was interpolated. Linear interpolation was performed to have everything in the same time scale. The model is written in Matlab code and runs in Matlab and the code runs in an EKF. This method was tested in order to try to solve the problem that the sensors come with different sampling time, see chapter 5. This method didn't work since there is a big risk that the data is destroyed, when its being linear interpolated before it is estimated by the EKF. A better method, which is used in this thesis and described in chapter 6, is to do a measurement update in the EKF every time a measurement comes.

10.2 Future work

More development work has to be done to improve the performance of the lane position monitoring system. An idea can be to integrate a spline model or a model made by toroids, for the purpose of building up the road, considering as an extra reference and giving better data to the lane positioning monitoring system.

More evaluation work for the parameters Q_k and R_k , both described in chapter 6 can be done, in order to give a more accurate position of the lane position monitoring system.

A graphical user interface can be implemented for the lane position monitoring system in order to give a better reference to a system that looks on drivers behaviour developed for drowsiness. The system is earlier made in a project, which is named Drowsi, where Volvo Technology participated among others.

Useful state and measurement equations from a positioning system with complete vehicle state model, described in [8], can be integrated into the extended model described in chapter 8. The gyroscope error model and the GPS error model in [8], can both for example be integrated in order to get an improvement of the estimated position by the EKF. The GPS error model, which is described in section 4.3 in [8], can be used to avoid errors.

Other improvements that can be made are if the camera can give more important information to the lane position monitoring system. It can for example be how the lines are drawn, the lines direction of travel, how many lines that are detected on the road. For example can such information be used if the camera detect lines cross the lane that information can be valuable as an extra reference telling the lane position monitoring system something is wrong. Other important information the camera can give are if bright lines are drawn on dark background such information can help the lane position monitoring system detect connected roads, crossings, roundabouts, tunnels, bridges and overtaking vehicles in order to get a more secure reference of the vehicle's position. That information can also be useful if the road has many lanes or if the road does not have any lines for the camera to measure. It can also be useful information for the lane position monitoring system when it snowing, raining or when there are changes of lights on the road for example when the vehicle is going under a bridge or through a tunnel.

Important improvements of the lane position monitoring system using additional sensor sources like map data and GPS that can be done, is to run data through Volvo's updated version of the map data program that also including more accurate maps than the ones that were used in this thesis, to evaluate the performance. Finally, more road attributes than curve radius from Volvo's map data program can be used to estimate the vehicle's position. For example the road attribute distance to next crossing can be used as a measurement signal in the extended model in chapter 8, in order to give a more accurate position of the lane position monitoring system.

Bibliography

- [1] Elliot D. Kaplan. *Understanding GPS: principles and applications*. Artech House, 1996.
- [2] Peter Hall. *A Bayesian Approach to Map-Aided Vehicle Positioning*. Linköping University Institute of Technology, 2001. LiTH-ISY-EX-3102.
- [3] www.navteq.com.
- [4] www.tomtom.com.
- [5] www.volvogroup.com.
- [6] Volvo Technology Corporation. 2010.
- [7] Y.Zhao. *Vehicle Location and Navigation Systems*. Artech House Publishers,Inc, Norwood, Great Britain, 1997.
- [8] David Andersson and Johan Fjellström. *Vehicle Positioning with Map Matching Using Integration of a Dead Reckoning System and GPS*. Linköping University Institute of Technology, 2004. LiTH-ISY-EX-3457-2004.
- [9] Andreas Eidehall. *Tracking and threat assessment for automotive collision avoidance*. Linköping University Institute of Technology, 2007. No. 1066.
- [10] Boucher C. Noyer J.-C. Lahrech, A. *Accurate vehicle positioning in urban areas*. Laboratoire d'Analyse des Systèmes du Littoral, Université du Littoral Côte d'Opale, 50 rue F. Buisson, BP 699, 62 228 Calais Cedex, France, 2005. 0-7803-9252-3.
- [11] Bonnifait Philippe Bétaille David Fouque, Clément. *Enhancement of Global Vehicle Localization using Navigable Road Maps and Dead-Reckoning*. HeuDiasyC UMR CNRS 6599, Université de Technologie de Compiègne, France, LCPC, Nantes, France, 2008. 1-4244-1537-3.
- [12] Christian Lundquist. *Sensor Fusion for Automotive Applications*. Linköping University Institute of Technology, 2011. No. 1409.

- [13] Hans Bohlin. *Integrationsmetoder för tröghetsnavigeringssystem och GPS*. Department of Electrical Engineering, Linköping University, Linköping, Sweden, 1994. LITH-ISY-EX-1398.
- [14] R. Behringer. <http://home.t-online.de/home/kontext/utm.htm>. volume 310 of Fortschrittsberichte VDI, Reihe 12. VDI Verlag, Düsseldorf Germany, 1997. Also as: PhD Thesis, Universität der Bundeswehr, 1996.
- [15] www.lantmateriet.se/geodesi/.
- [16] Arnold Andreasson. <http://mellifica.se/konsult>. 2007.
- [17] Björn Sällarp. <http://blog.sallarp.com>. License: <http://creativecommons.org/licenses/by-nc-sa/3.0/> public class GaussKreuger, 2009.
- [18] M. Macnaughtan C. Drane and C. Scott. *Positioning GSM telephones*. IEEE Communications Magazine, 36(4), Computer Systems Engineering University of Technology, Sydney, Australia, April 1998.
- [19] Jay Farrell and Matthew Barth. *The Global Positioning System and Inertial Navigation*. McGraw-Hill, New York, USA, 1998.
- [20] Richard Hartley and Andrew Zisserman. *Multiple View Geometry in Computer Vision*. Cambridge University Press, 2 edition, 3 2004.
- [21] Henrik Stewénius Chris Engels and David Nistér. Bundle adjustment rules. *Photogrammetric Computer Vision*, 2, 2006.
- [22] Motilal Agrawal Kurt Konolige and Joan Solà. Large-scale visual odometry for rough terrain. *Robotics Research*, 2011.
- [23] Jonas Fredriksson Jonas Nilsson and Anders C.E. Ödblom. Bundle adjustment using single-track vehicle model. *IEEE International Conference on Robotics and Automation (ICRA)*, pages 2888 – 2893, 5 2013.
- [24] Per-Johan Nordlund. *En simuleringsmiljö för tröghetsnavigering samt en metod för integration av tröghetsnavigeringssystem och GPS*. Master's thesis LiTH-ISY-EX-1728, Department of Electrical Engineering, Linköping University, Linköping, Sweden, December 1996.
- [25] Ralf Raimann. *VT LPS Performance Specification*. Internal document at Volvo Technology Corporation, 2003. Document number: 10096047.
- [26] Garmin. *GPS 18 Technical Specifications*. Garmin International, Inc., june 2005. 190-00307-00.
- [27] Anders Karlsson. *Integration of map data for truck applications*. Volvo Technology, Dept. 6320 M1.6, Götaverksgatan 10, 405 08 Göteborg, Sweden, 9 2009.

- [28] Per Nordqvist. *GPSToRoute documentation*. Volvo Technology Corporation, Dept. 6350 M1.6, Götaverksgatan 10, 405 08 Göteborg, Sweden, 2010.
- [29] Fredrik Gustafsson. *Statistical Sensor Fusion*. Studentlitteratur AB, Lund, 2010. ISBN 978-91-44-05489-6.
- [30] Fredrik Gustafsson, Lennart Ljung, and Mille Millnert. *Signalbehandling*. Studentlitteratur AB, Lund, 2009. ISBN 978-91-44-01709-9.
- [31] Fredrik Gustafsson. Particle filter theory and practice with positioning applications. *Aerospace and Electronic Systems Magazine, IEEE*, 25:53–82, 7 2010.
- [32] S.J. Julier, J.K. Uhlmann, and H.F. Durrant-Whyte. A new approach for filtering nonlinear systems. In *Proceedings of the American Control Conference*, vol.3:1628–1632, 1995.
- [33] S.J. Julier, J.K. Uhlmann, and H.F. Durrant-Whyte. Unscented filtering and nonlinear estimation. *Proceedings of IEEE*, 92:401–422, 3 (Mar.2004).
- [34] Magnus Noorgard, Niels K. Poulsen, and Ole Ravn. New developments in state estimation of nonlinear systems. *Automatica*, 36:1627–1638, 2000.
- [35] Daniel L. Alspach and Harold W. Sorenson. Nonlinear bayesian estimation using gaussian sum approximations. *IEEE Transaction on Automatic Control*, 17:439–448, 1972.
- [36] Haykin S. Arasaratnam, I. and R. Elliot. Discrete-time nonlinear filtering algorithms using gauss-hermite quadrature. *Proceedings of IEEE*, 95:953–977, 2007.
- [37] Stuart C. Kramer and Harold W. Sorenson. Recursive bayesian estimation using piece-wise constant. *Automatica*, 24:789–801, 1988.
- [38] Christian Lundquist. *Automotive Sensor Fusion for Situation Awareness*. Linköping University Institute of Technology, 2009. No. 1422.
- [39] Ernst D. Dickmanns. *Dynamic Vision for Perception and Control of Motion*. Springer-Verlag, 2007. ISBN 978-1-84628-637-7.
- [40] R. Behringer. *Visuelle Erkennung und Interpretation des Fahrspurverlaufes durch Rechnersehen für ein autonomes Strassenfahrzeug*. volume 310 of Fortschrittsberichte VDI, Reihe 12. VDI Verlag, Düsseldorf Germany, 1997. Also as: PhD Thesis, Universität der Bundeswehr, 1996.
- [41] Torkel Glad Lennart Ljung. *Modellbygge och Simulering*. Studentlitteratur, 2 edition, 2004. ISBN 978-91-44-02443-1.

Appendix A

Figures

A.1 The raw signal for the whole route

In this section figures of the raw signal for the whole route are shown to give a better understanding of the signal's behaviour and characteristics.

A.1.1 Data from GPS

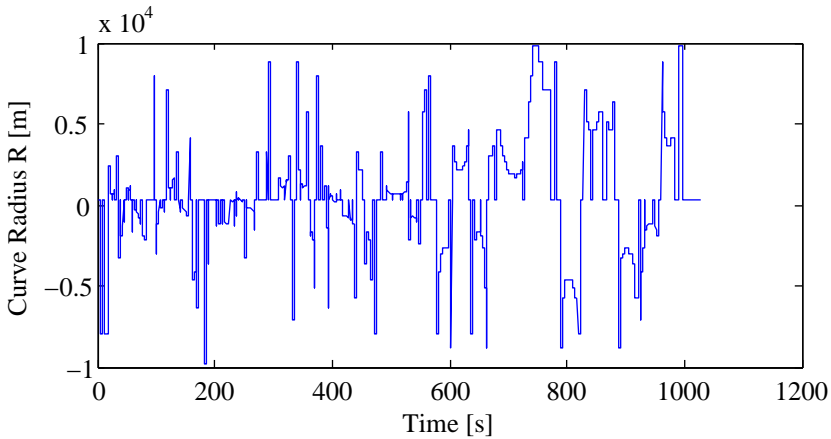


Figure A.1. Raw signal: Curve radius from map data

A.1.2 Data from the Swedish National Road Administration

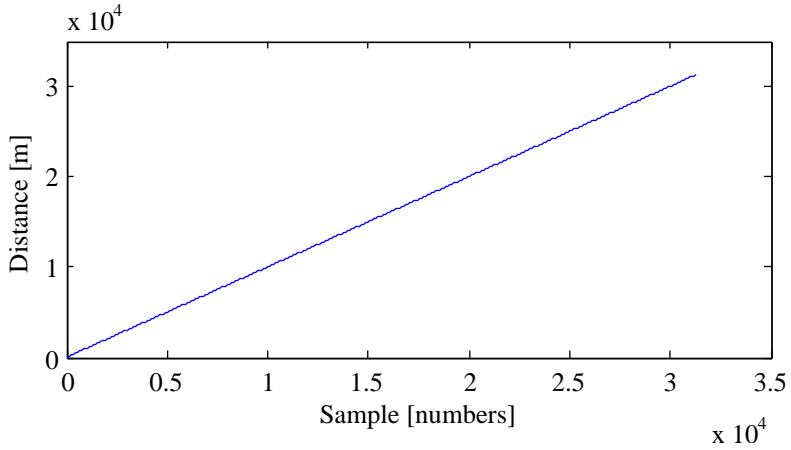


Figure A.2. Raw signal: Distance from Vägverket

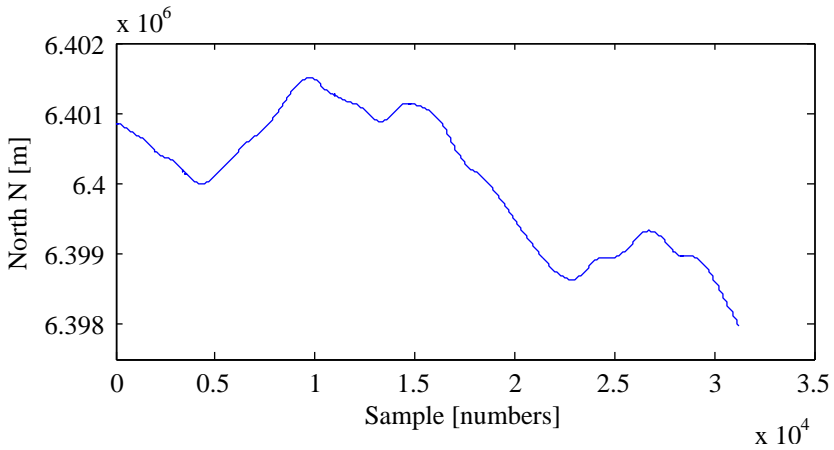


Figure A.3. Raw signal: x-coordinate of GPS in RT90 from Vägverket

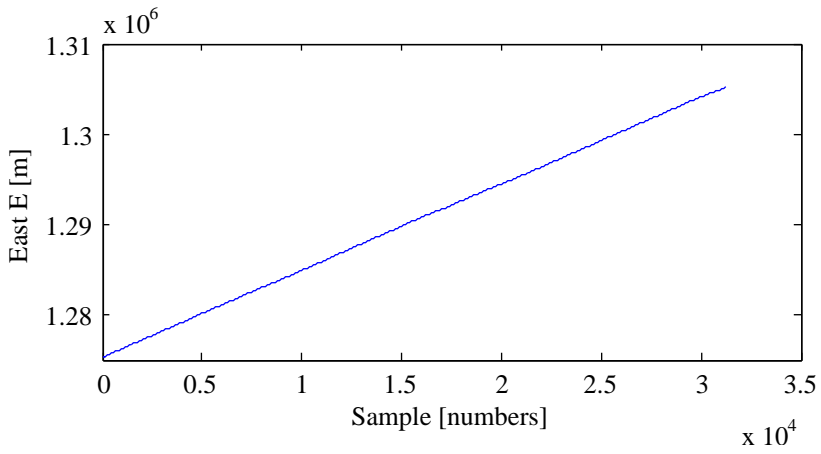


Figure A.4. Raw signal: y-coordinate of GPS in RT90 from Vägverket

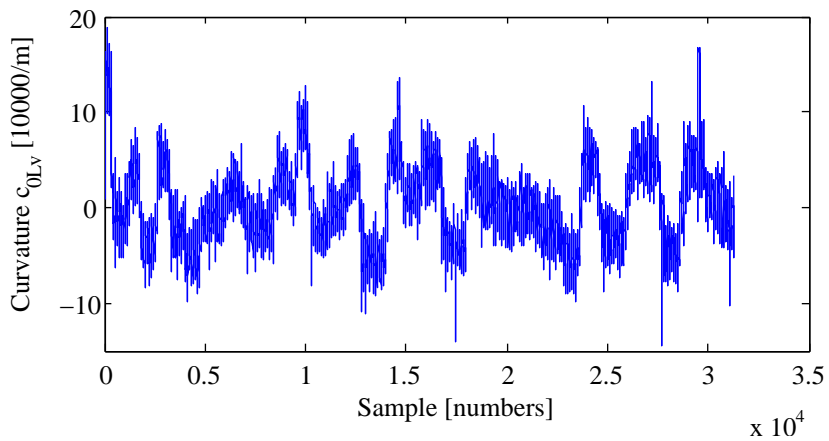


Figure A.5. Raw signal: Curvature from Vägverket

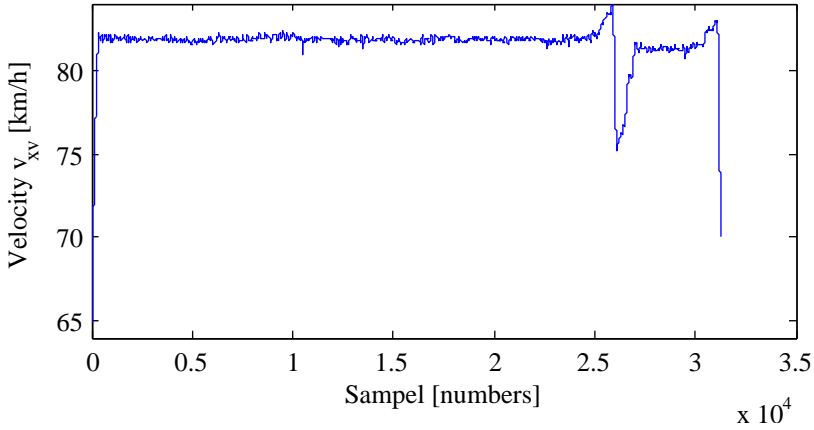


Figure A.6. Raw signal: Longitudinal velocity from Vägverket

A.2 The raw signal on a selected interval for the whole route on a road stretch with curves

A.2.1 Data from LPS system on a road stretch with curves

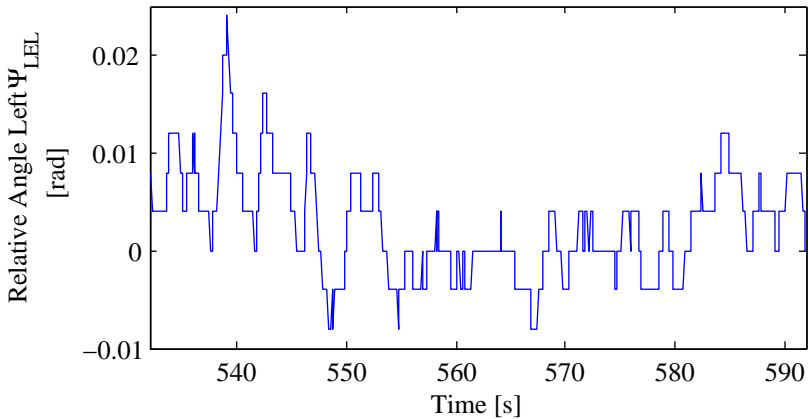


Figure A.7. Raw signal: Relative angle left between vehicle and road on a road stretch with curves

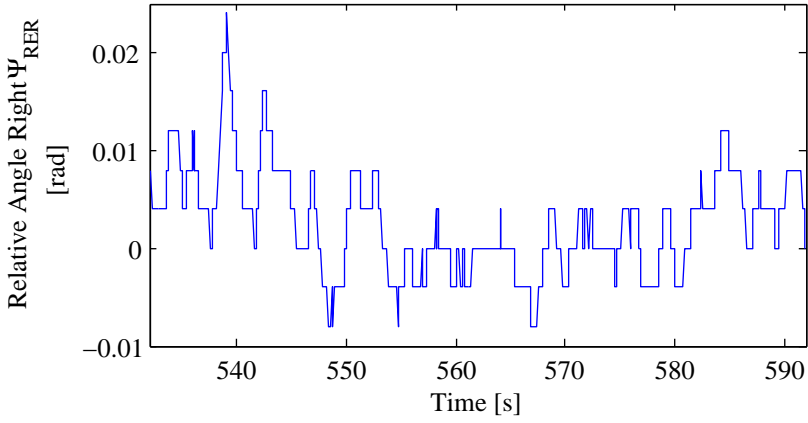


Figure A.8. Raw signal: Relative angle right between vehicle and road on a road stretch with curves

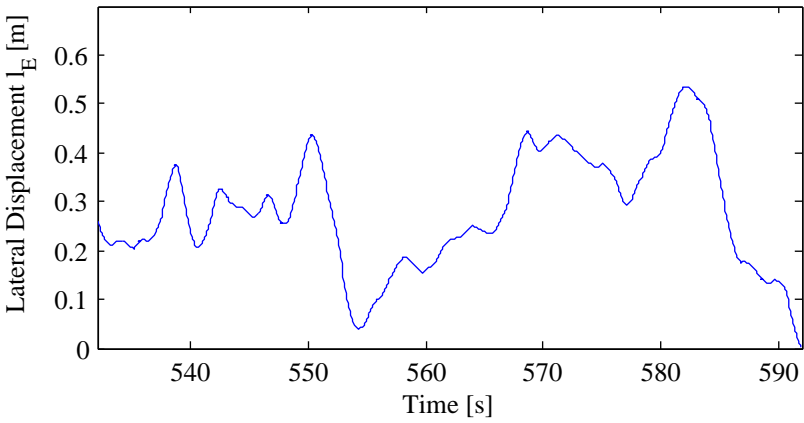


Figure A.9. Raw signal: Lateral displacement of vehicle in lane on a road stretch with curves

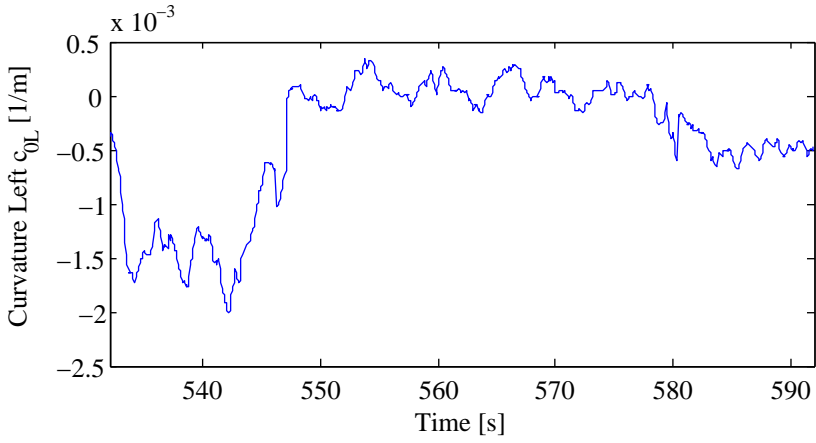


Figure A.10. Raw signal: Curvature from LPS system left on a road stretch with curves

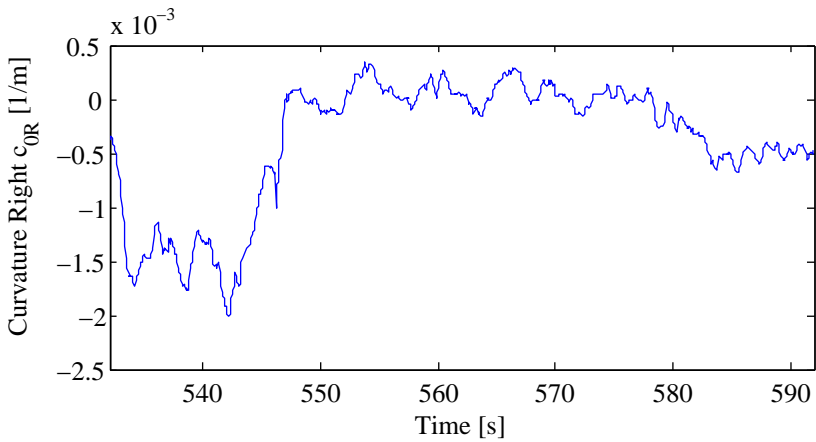


Figure A.11. Raw signal: Curvature from LPS system right on a road stretch with curves

A.2.2 Data from vehicle sensors

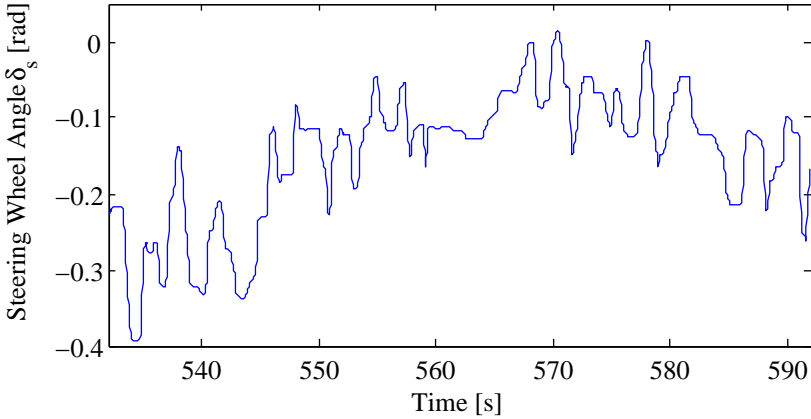


Figure A.12. Raw signal: Steering wheel angle on a road stretch with curves

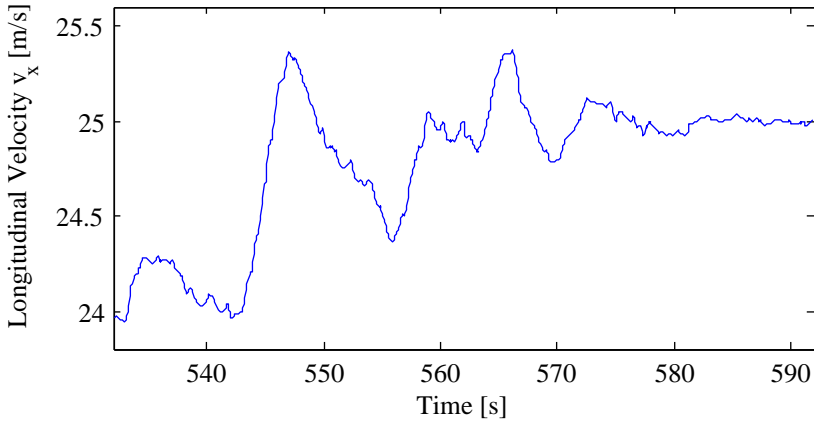


Figure A.13. Raw signal: Longitudinal velocity on a road stretch with curves

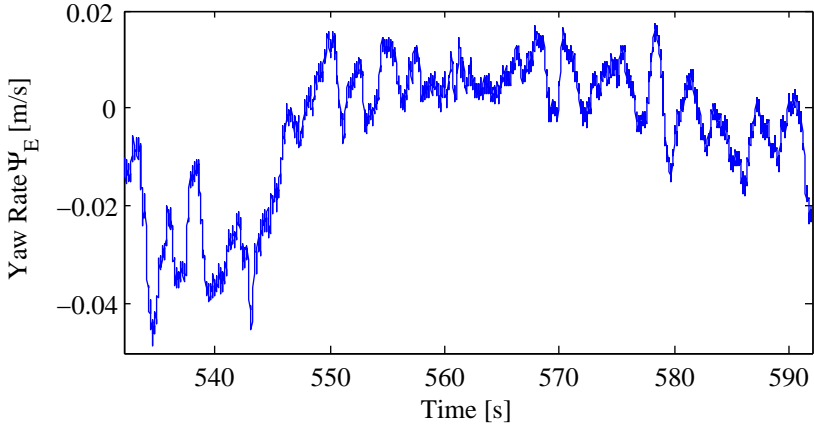


Figure A.14. Raw signal: Yaw Rate on a road stretch with curves

A.2.3 Data from GPS

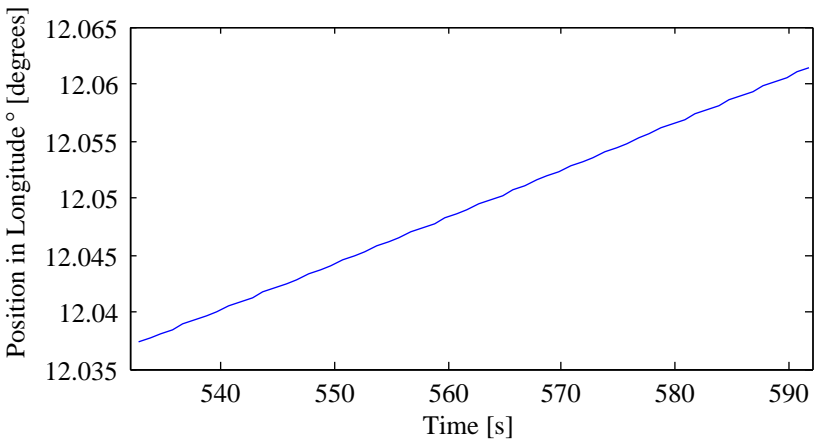


Figure A.15. Raw signal: x-coordinate of GPS in WGS 84 on a road stretch with curves

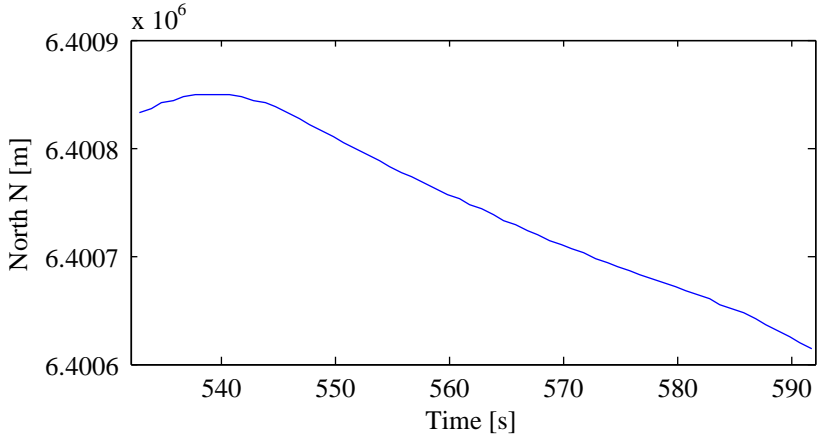


Figure A.16. Raw signal: x-coordinate of GPS in RT90 on a road stretch with curves

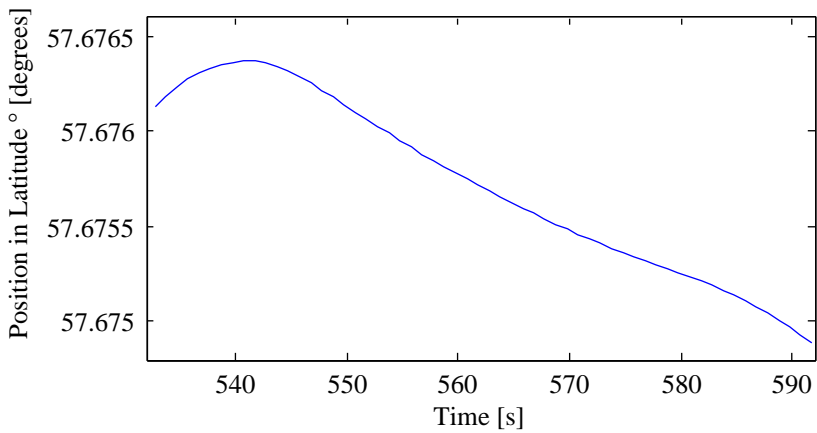


Figure A.17. Raw signal: y-coordinate of GPS in WGS 84 on a road stretch with curves

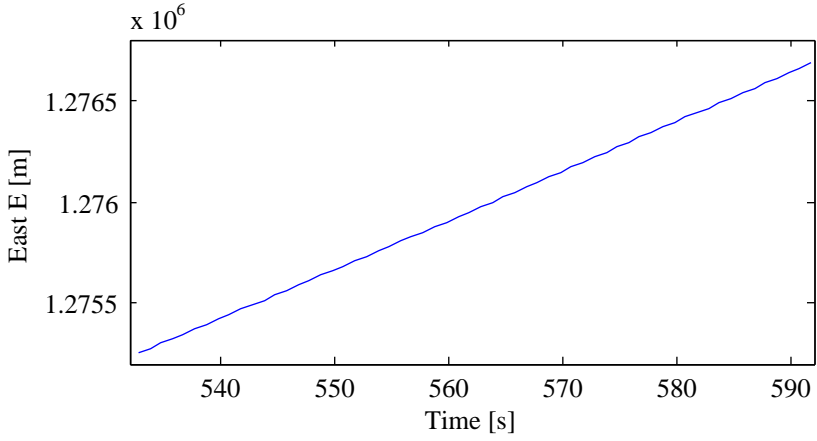


Figure A.18. Raw signal: y-coordinate of GPS in RT90 on a road stretch with curves

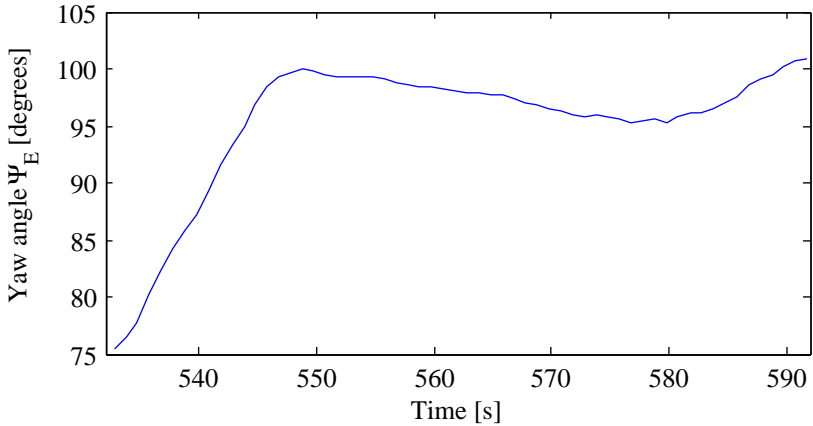


Figure A.19. Raw signal: The ego vehicle's yaw angle on a road stretch with curves

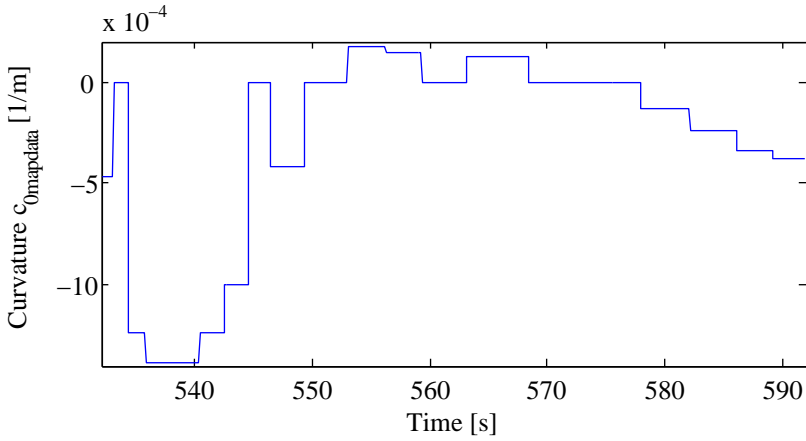


Figure A.20. Raw signal: Curvature from map data on a road stretch with curves

A.3 The raw signal on a selected interval for the whole route with disturbance

A.3.1 Data from LPS system

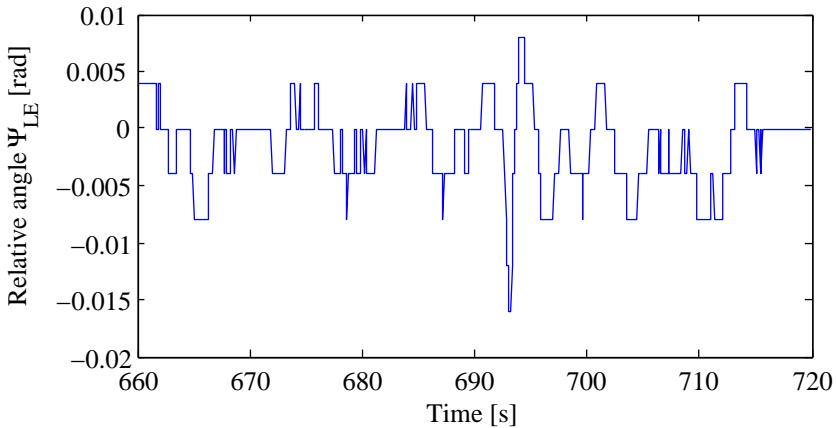


Figure A.21. Raw signal: Relative angle left between vehicle and road on a road stretch with slight curves with disturbance

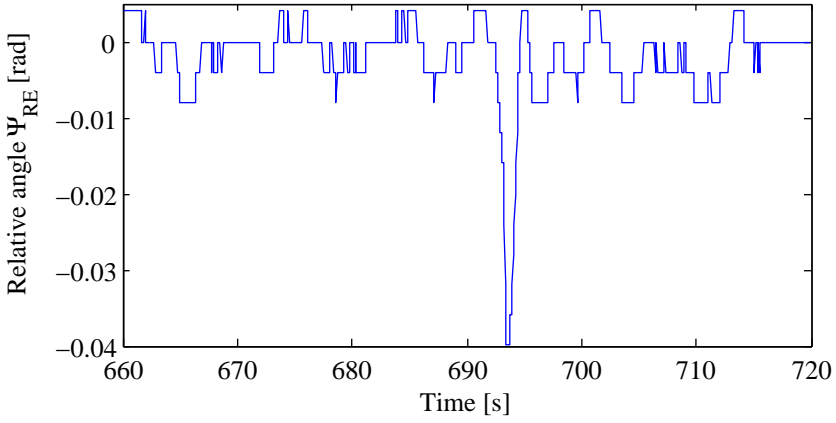


Figure A.22. Raw signal: Relative angle right between vehicle and road on a road stretch with slight curves with disturbance

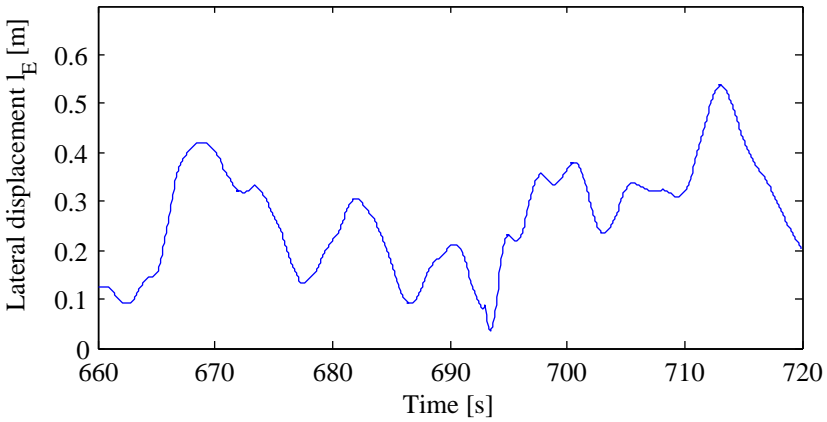


Figure A.23. Raw signal: Lateral displacement of vehicle in lane on a road stretch with slight curves with disturbance

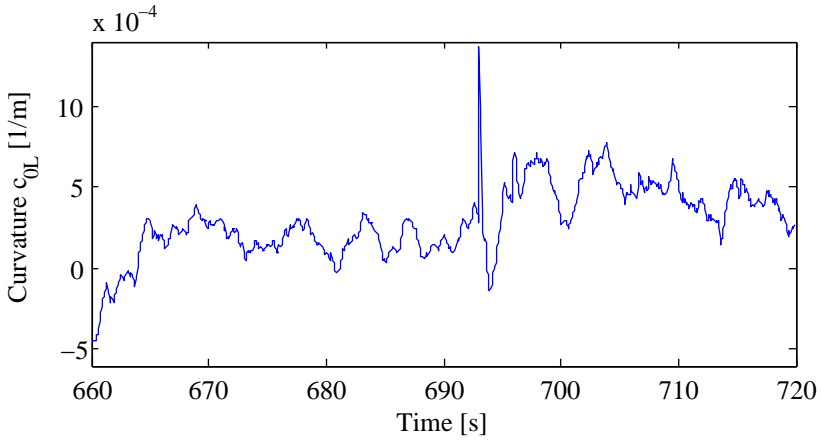


Figure A.24. Raw signal: Curvature from LPS system left on a road stretch with slight curves with disturbance

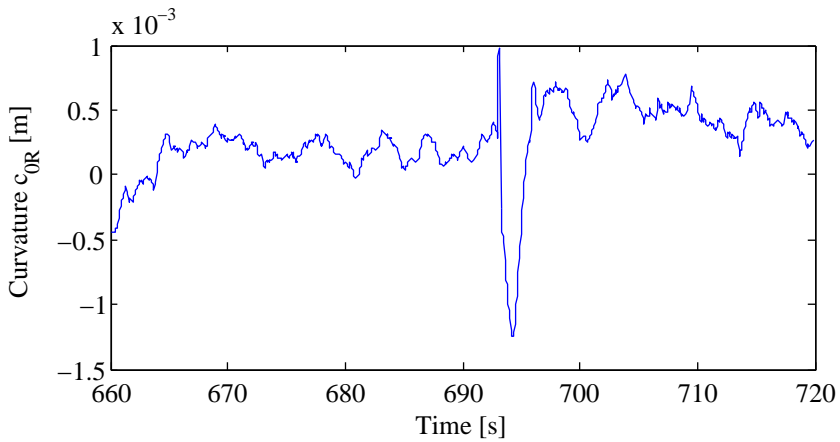


Figure A.25. Raw signal: Curvature from LPS system right on a road stretch with slight curves with disturbance

A.3.2 Data from vehicle sensors

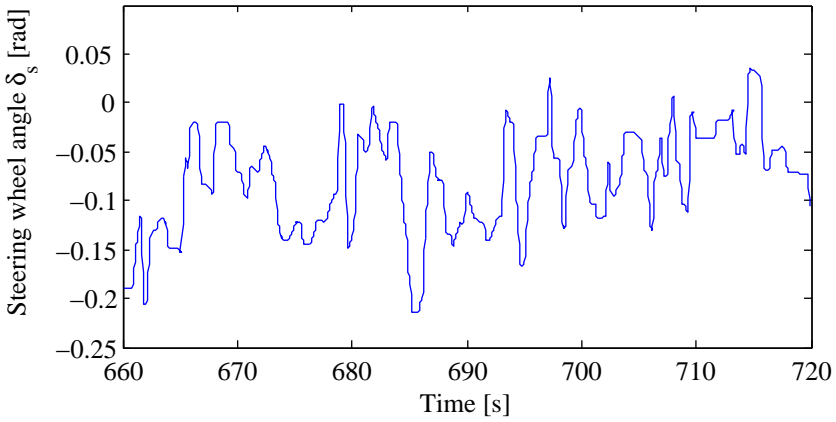


Figure A.26. Raw signal: Steering wheel angle on a road stretch with slight curves with disturbance

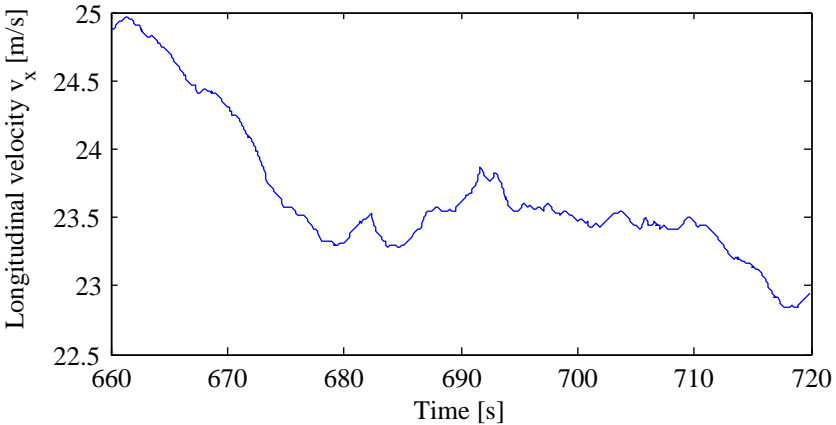


Figure A.27. Raw signal: Longitudinal velocity on a road stretch with slight curves with disturbance

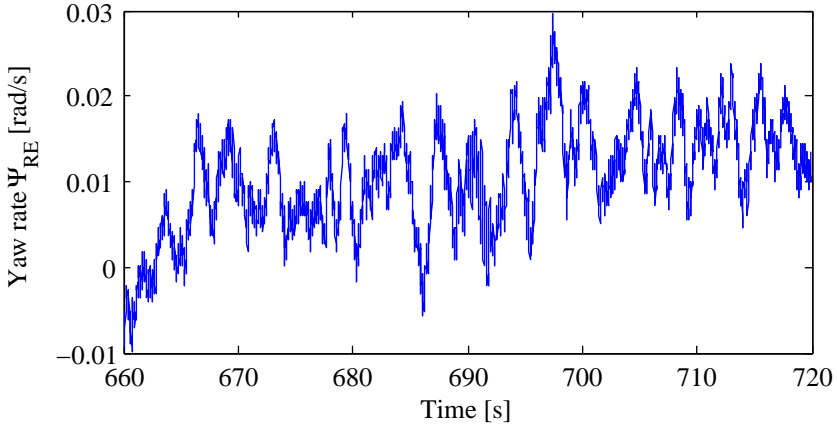


Figure A.28. Raw signal: Yaw Rate on a road stretch with slight curves with disturbance

A.3.3 Data from GPS

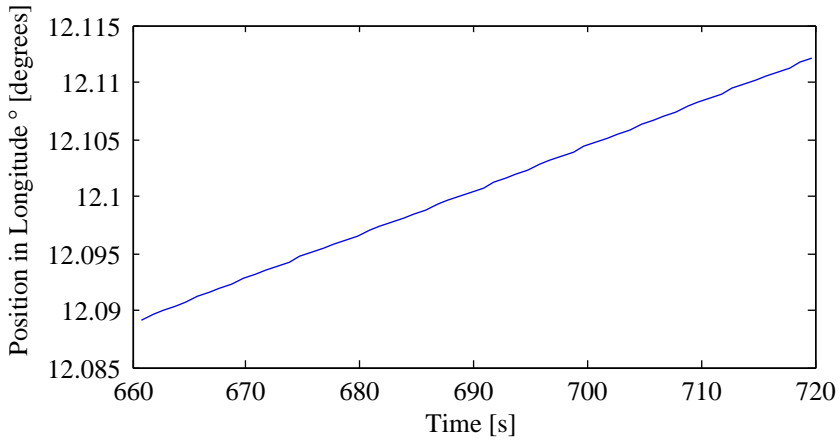


Figure A.29. Raw signal: x-coordinate of GPS in WGS 84 on a road stretch with slight curves with disturbance

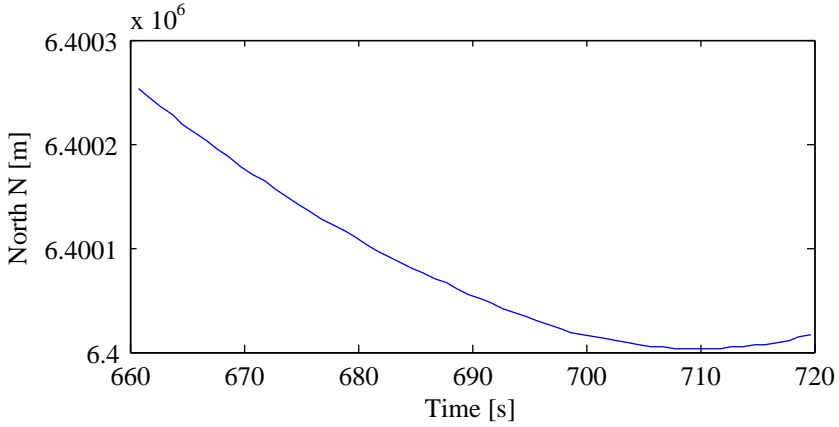


Figure A.30. Raw signal: x-coordinate of GPS in RT90 on a road stretch with slight curves with disturbance

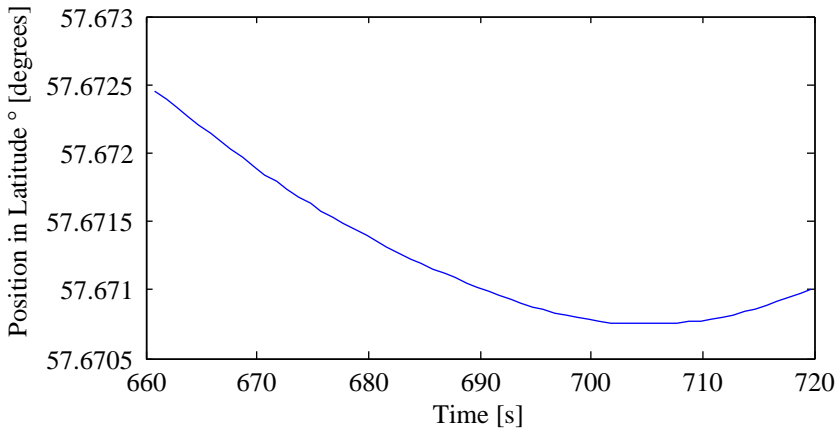


Figure A.31. Raw signal: y-coordinate of GPS in WGS 84 on a road stretch with slight curves with disturbance

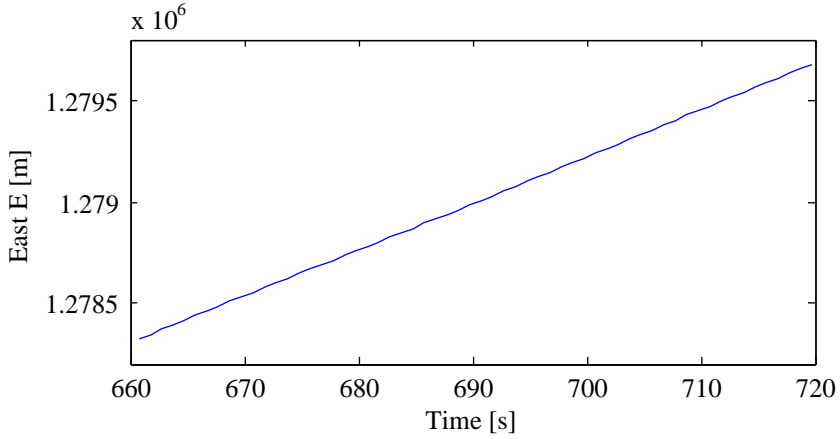


Figure A.32. Raw signal: y-coordinate of GPS in RT90 on a road stretch with slight curves with disturbance

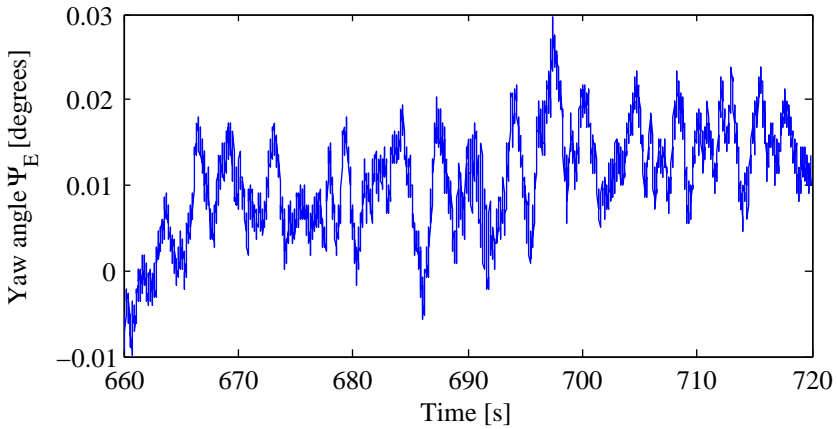


Figure A.33. Raw signal: The ego vehicle's yaw angle on a road stretch with slight curves with disturbance

Appendix B

Figures from technique 4, chapter 9.4

B.1 Technique 4

In this appendix figures from technique 4, chapter 9.4 are presented.

B.1.1 Subtechnique T4GPS

Here figures from subtechnique T4GPS, chapter 9.4 are provided.

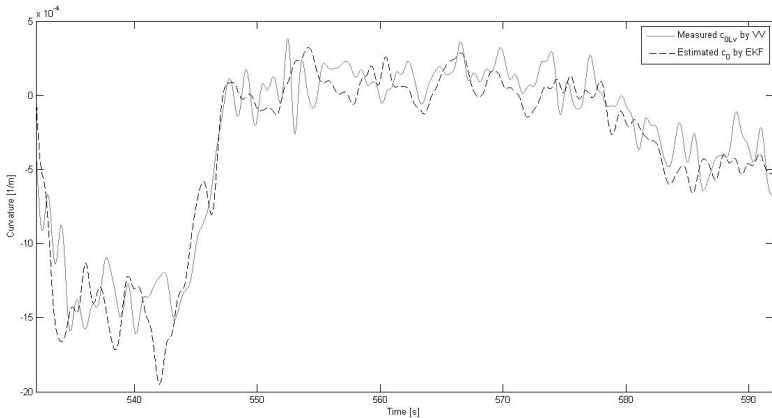


Figure B.1. Comparison between the measured curvature from SNRA c_{0LV} (gray) and the estimated curvature without map data from the EKF c_0 (black dashed) for Data sequence 1, as described in chapter 5.1.1 and according to technique 4. Note that the scale is very small ($1 * 10^{-4}$), resulting in small changes in time have a large effect in the curvature.

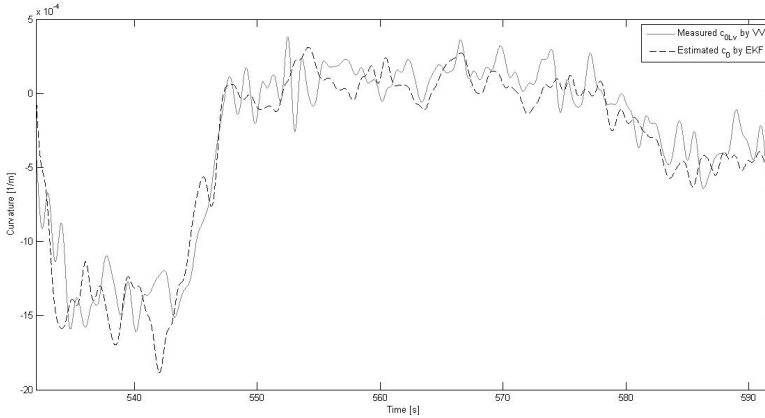


Figure B.2. Comparison between the measured curvature from SNRA c_{0LV} (gray) and the estimated curvature with map data from the EKF c_0 (black dashed) for Data sequence 1, as described in chapter 5.1.1 and according to technique 4. Note that the scale is very small ($1 * 10^{-4}$), resulting in small changes in time have a large effect in the curvature.

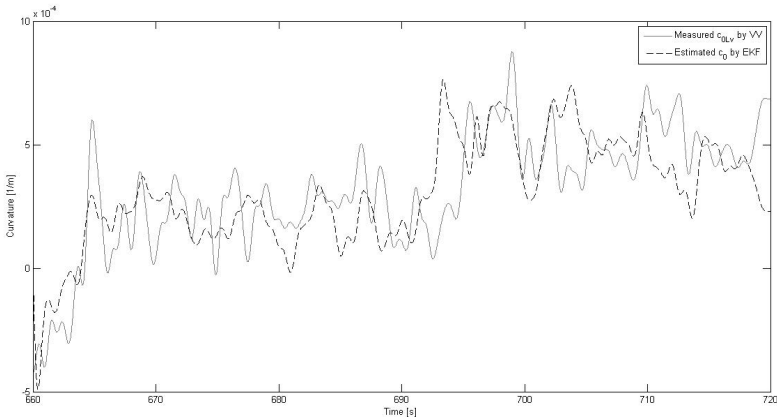


Figure B.3. Comparison between the measured curvature from SNRA c_{0LV} (gray) and the estimated curvature without map data from the EKF c_0 (black dashed) for Data sequence 1, as described in chapter 5.1.1 and according to technique 4. Note that the scale is very small ($1 * 10^{-4}$), resulting in small changes in time have a large effect in the curvature.

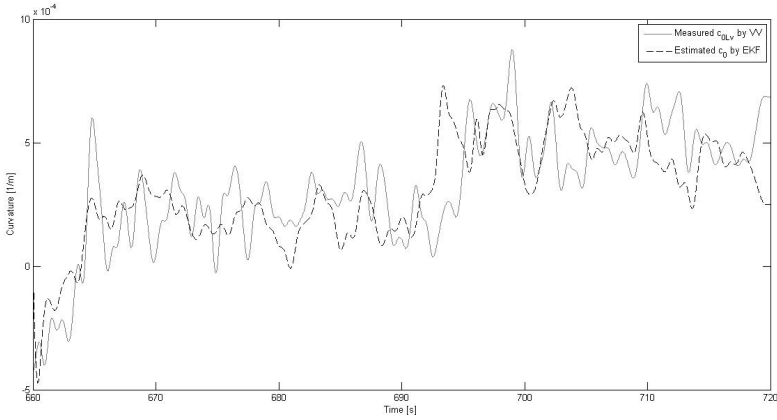


Figure B.4. Comparison between the measured curvature from SNRA c_{0LV} (gray) and the estimated curvature with map data from the EKF c_0 (black dashed) for Data sequence 1, as described in chapter 5.1.1 and according to technique 4. Note that the scale is very small ($1 * 10^{-4}$), resulting in small changes in time have a large effect in the curvature.

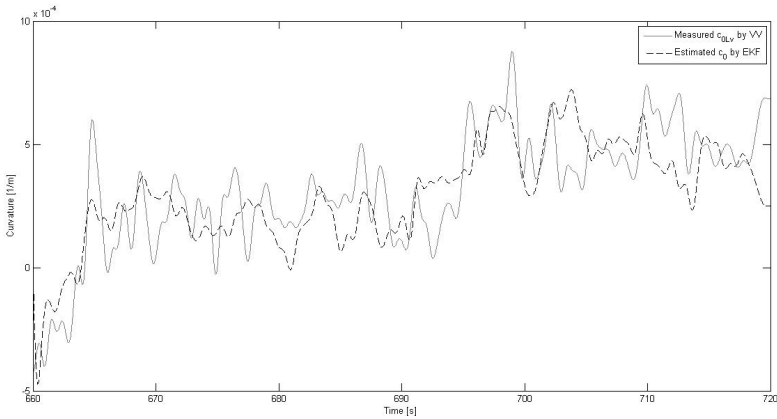


Figure B.5. Comparison between the measured curvature from SNRA c_{0LV} (gray) and the estimated curvature with map data and reliable camera data from the EKF c_0 (black dashed) for Data sequence 1, as described in chapter 5.1.1 and according to technique 4. Note that the scale is very small ($1 * 10^{-4}$), resulting in small changes in time have a large effect in the curvature.

B.1.2 Subtechnique T4Distance

The figures of subtechnique T4Distance, chapter 9.4 are here presented.

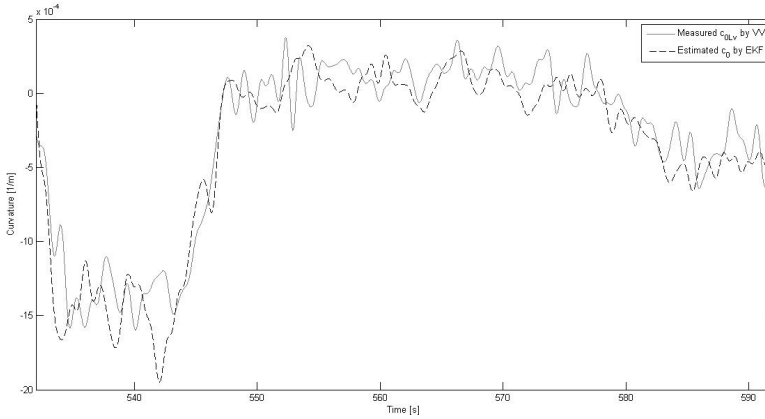


Figure B.6. Comparison between the measured curvature from SNRA c_{0LV} (gray) and the estimated curvature without map data from the EKF c_0 (black dashed) for Data sequence 1, as described in chapter 5.1.1 and according to technique 4. Note that the scale is very small ($1 * 10^{-4}$), resulting in small changes in time have a large effect in the curvature.

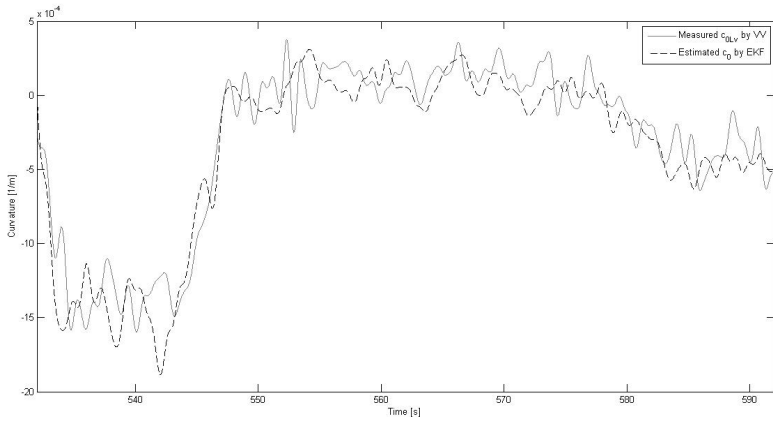


Figure B.7. Comparison between the measured curvature from SNRA c_{0LV} (gray) and the estimated curvature with map data from the EKF c_0 (black dashed) for Data sequence 1, as described in chapter 5.1.1 and according to technique 4. Note that the scale is very small ($1 * 10^{-4}$), resulting in small changes in time have a large effect in the curvature.

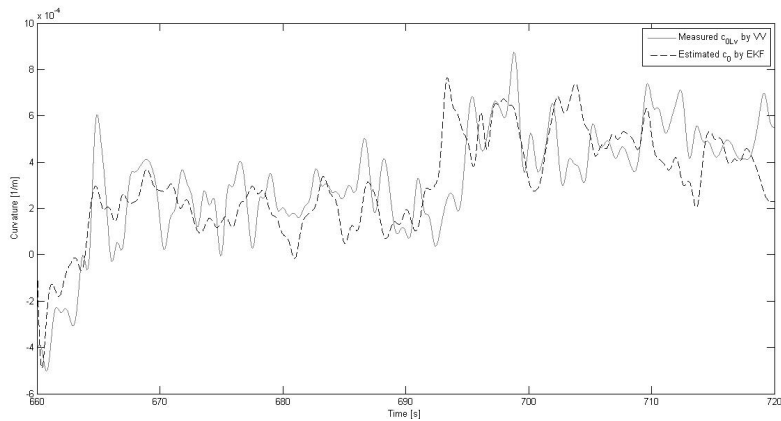


Figure B.8. Comparison between the measured curvature from SNRA c_{0LV} (gray) and the estimated curvature without map data from the EKF c_0 (black dashed) for Data sequence 1, as described in chapter 5.1.1 and according to technique 4. Note that the scale is very small ($1 * 10^{-4}$), resulting in small changes in time have a large effect in the curvature.

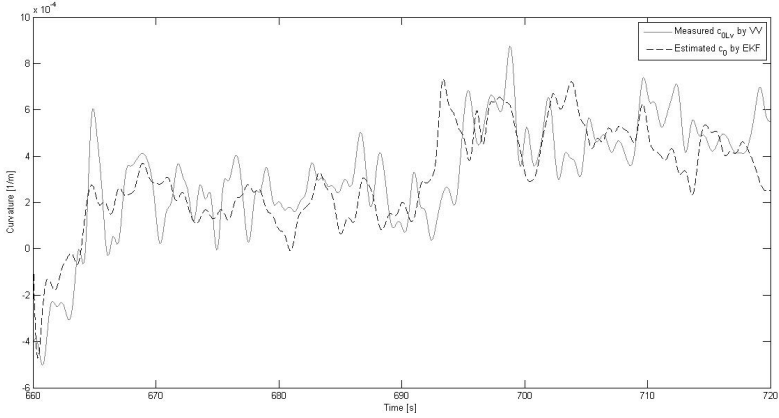


Figure B.9. Comparison between the measured curvature from SNRA c_{0LV} (gray) and the estimated curvature with map data from the EKF c_0 (black dashed) for Data sequence 1, as described in chapter 5.1.1 and according to technique 4. Note that the scale is very small ($1 * 10^{-4}$), resulting in small changes in time have a large effect in the curvature.

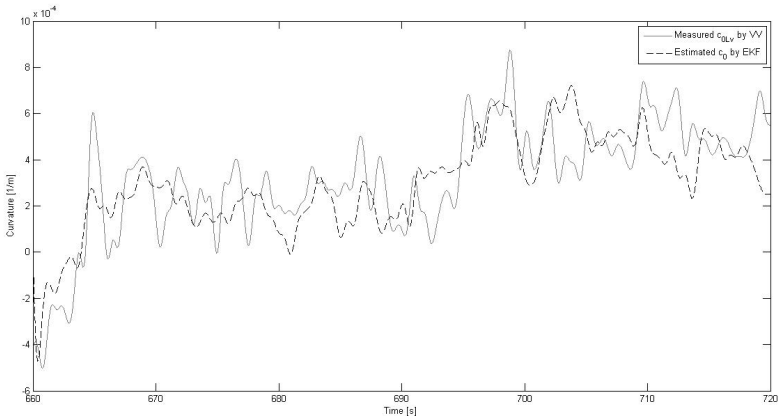


Figure B.10. Comparison between the measured curvature from SNRA c_{0LV} (gray) and the estimated curvature with map data and reliable camera data from the EKF c_0 (black dashed) for Data sequence 1, as described in chapter 5.1.1 and according to technique 4. Note that the scale is very small ($1 * 10^{-4}$), resulting in small changes in time have a large effect in the curvature.

B.1.3 Subtechnique T4Time

Figures from subtechnique T4Time, chapter 9.4 are shown here.

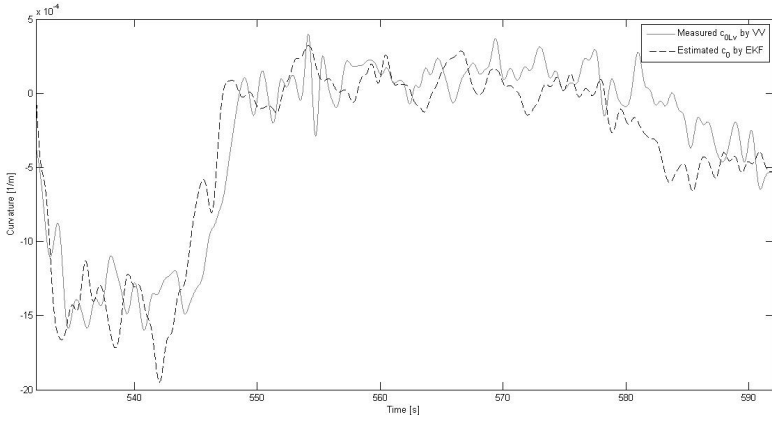


Figure B.11. Comparison between the measured curvature from SNRA c_{0LV} (gray) and the estimated curvature without map data from the EKF c_0 (black dashed) for Data sequence 1, as described in chapter 5.1.1 and according to technique 4. Note that the scale is very small ($1 * 10^{-4}$), resulting in small changes in time have a large effect in the curvature.

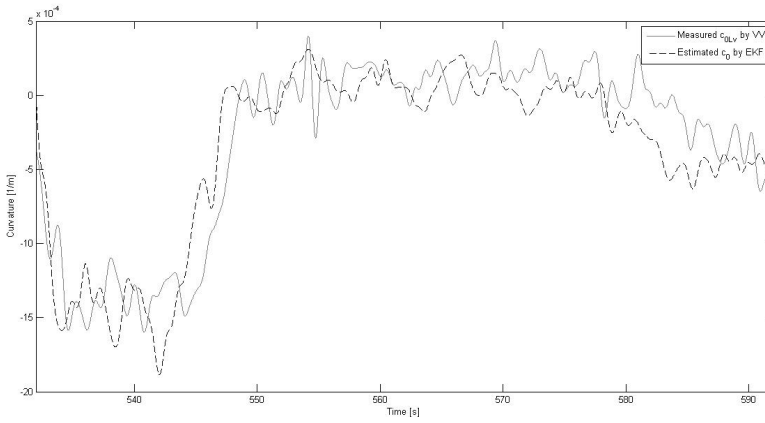


Figure B.12. Comparison between the measured curvature from SNRA c_{0LV} (gray) and the estimated curvature with map data from the EKF c_0 (black dashed) for Data sequence 1, as described in chapter 5.1.1 and according to technique 4. Note that the scale is very small ($1 * 10^{-4}$), resulting in small changes in time have a large effect in the curvature.

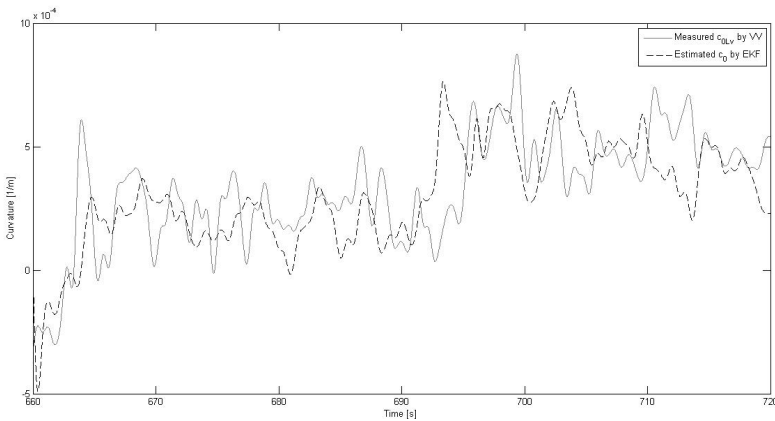


Figure B.13. Comparison between the measured curvature from SNRA c_{0LV} (gray) and the estimated curvature without map data from the EKF c_0 (black dashed) for Data sequence 1, as described in chapter 5.1.1 and according to technique 4. Note that the scale is very small ($1 * 10^{-4}$), resulting in small changes in time have a large effect in the curvature.

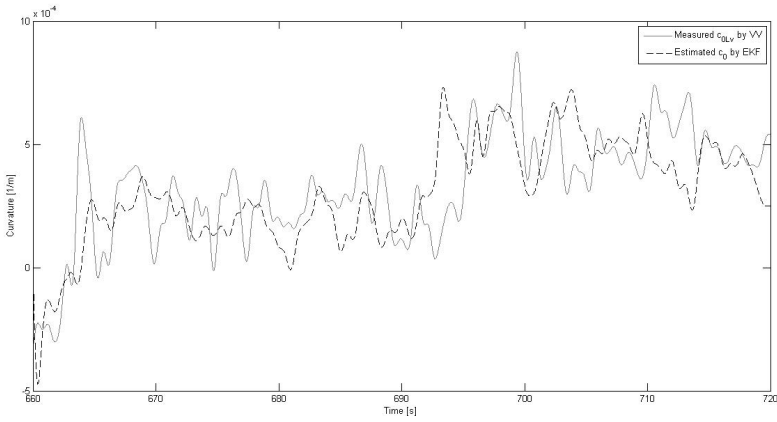


Figure B.14. Comparison between the measured curvature from SNRA c_{0LV} (gray) and the estimated curvature with map data from the EKF c_0 (black dashed) for Data sequence 1, as described in chapter 5.1.1 and according to technique 4. Note that the scale is very small ($1 * 10^{-4}$), resulting in small changes in time have a large effect in the curvature.

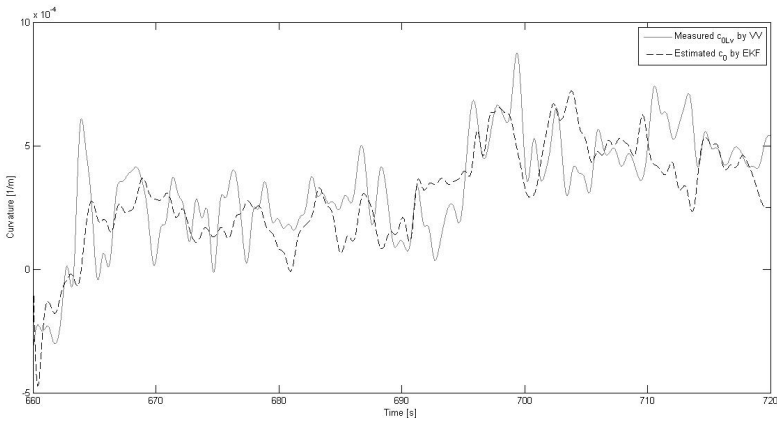


Figure B.15. Comparison between the measured curvature from SNRA c_{0LV} (gray) and the estimated curvature with map data and reliable camera data from the EKF c_0 (black dashed) for Data sequence 1, as described in chapter 5.1.1 and according to technique 4. Note that the scale is very small ($1 * 10^{-4}$), resulting in small changes in time have a large effect in the curvature.